PERGAMON

International Journal of Hydrogen Energy 27 (2002) 991–1022

International Journal of HYDROGEN ENERGY

www.elsevier.com/locate/ijhydene

Review Article

Photo-electrochemical hydrogen generation from water using solar energy. Materials-related aspects

T. Bak, J. Nowotny *, M. Rekas, C.C. Sorrell

Centre for Materials Research in Energy Conversion, School of Materials Science and Engineering, The University of New South Wales, Sydney, NSW 2052, Australia

Abstract

The present work considers hydrogen generation from water using solar energy. The work is focused on the materials-related issues in the development of high-efficiency photo-electrochemical cells (PECs). The property requirements for photo-electrodes, in terms of semiconducting and electrochemical properties and their impact on the performance of PECs, are outlined. Different types of PECs are overviewed and the impact of the PEC structure and materials selection on the conversion efficiency of solar energy are considered.

Trends in research in the development of high-efficiency PECs are discussed. It is argued that very sophisticated materials engineering must be used for processing the materials that will satisfy the specific requirements for photo-electrodes. An important issue in the processing of these materials is the bulk vs. interface properties at the solid/solid interfaces (e.g., grain boundaries) and solid/liquid interfaces (e.g., electrode/electrolyte interface). Consequently, the development of PECs with the efficiency required for commercialization requires the application of up-to-date materials processing technology.

The performance of PECs is considered in terms of:

- excitation of electron–hole pair in photo-electrodes;
- charge separation in photo-electrodes;
- electrode processes and related charge transfer within PECs;
- generation of the PEC voltage required for water decomposition.

This work also gives empirical data on the performance of PECs of different structures and materials selection.

It is argued that PEC technology is the most promising technology for hydrogen production owing to several reasons:

- PEC technology is based on solar energy, which is a perpetual source of energy, and water, which is a renewable resource;
- PEC technology is environmentally safe, with no undesirable byproducts;
- PEC technology may be used on both large and small scales;
- PEC technology is relatively uncomplicated.

According to current predictions, the production of hydrogen will skyrocket by 2010 (Morgan and Sissine, Congressional Research Service, Report for Congress. The Committee for the National Institute for the Environment, Washington, DC, 20006-1401, 28 April 1995). Consequently, seed funding already has been allocated to several national research programs aiming at the development of hydrogen technology. The countries having access to this PEC technology are likely to form the OPEC of the future.

Keywords: Hydrogen generation; Photo-electrodes; Solar energy conversion; Photo-electrochemistry; Photo-cells; Semiconducting materials

*Tel.: +61-2-9385-6465; fax: +61-2-9385-6467.
E-mail address: j.nowotny@unsw.edu.au (J. Nowotny).

0360-3199/02/$ 22.00
PII: S0360-3199(02)00022-8

Contents

1. Introduction

1.1. Hydrogen: fuel of the future

Hydrogen is widely considered to be the fuel of the future. Consequently, there have been intensive efforts in the development of different technologies based on the applications of hydrogen as a fuel instead of fossil fuels owing to the following reasons:

- the use of fossil fuels is responsible for climate change [1–5];
- deposits of fossil fuels are limited;
- the price of the fossil fuels is increasing;
- there is a need for a fuel generated from the raw materials which are abundantly available;
- there is a need for a fuel that is environmentally safe.

Hydrogen has many potential applications, including the powering of nonpolluting vehicles, domestic heating, and aircraft. Therefore, hydrogen, as an energy carrier, is anticipated to join photovoltaic electricity as the foundation of sustainable energy system [1,2,6]. Recent efforts in the development of vehicles fuelled by hydrogen, either directly or through hydrogen fuel cells, may serve as examples of

Nomenclature

A	irradiated area (m^2)
a	Anode/photo-anode
AM	air mass
c	speed of light in vacuo (2.99793×10^8 m/s)
c	cathode/photo-cathode
Dye	photo-sensitizer at ground state
Dye^*	dye at excited state
Dye^+	dye at charged state
e	elementary charge (1.602×10^{-19} C)
e′	quasi-free electron
E	energy (eV)
E_B	potential energy related to the bias ($E_B = eV_{bias}$)
E_c	energy of the bottom of the conduction band (eV)
E_F	Fermi energy (eV)
E_g	band gap (eV)
E_i	threshold energy (eV)
$E(H^+/H_2)$	energy of the redox couple H^+/H_2 (eV)
$E(O_2/H_2O)$	energy of the redox couple O_2/H_2O (eV)
E_{loss}	energy loss (eV)
E_l	electrolyte
$E_{n,d}$	free enthalpy of electrochemical oxidation (per one electron hole) (eV)
$E_{p,d}$	free enthalpy of electrochemical reduction (per one electron) (eV)
E_v	energy of the top of the valence band (eV)
EMF	electromotive force (open circuit voltage) (V)
F	Faraday constant ($F = eN_A$) (9.648×10^4 C mol^{-1})
G	Gibbs energy (free enthalpy) (kJ mol^{-1})
G^0	standard Gibbs energy (standard free enthalpy) (kJ mol^{-1})
ΔG_a	free enthalpy of anodic decomposition (kJ mol^{-1})
ΔG_c	free enthalpy of cathodic decomposition (kJ mol^{-1})
ΔG_{loss}	free energy losses related with anodic and cathodic over-potentials
$\Delta G(H_2O)$	free energy of H_2O formation
h	Planck constant (6.626×10^{-34} J s)
$h^{\cdot}$	quasi-free electron hole
H^+	hydrogen ion (can be considered as hydronion ion H_3O^+)
HPE	hybrid photo-electrode
I	current (A)
IPCE	incident photon-to-current efficiency
I_r	incidence of solar irradiance (W m^{-2})
i	concentration of ionic charge carriers (cm^{-3})
J	flux density (amount of some quantity flowing across a given area—often unit area perpendicular to the flow—per unit time, e.g. number of particles) (m^{-2} s^{-1})
J_g	flux density of absorbed photons (m^{-2} s^{-1})
M	metal
MO_x	metal oxide (x corresponds to oxygen stoichiometry)
N	number of photons
N_A	Avogadro number (6.022×10^{23} mol^{-1})
N_{eff}	efficient number of incidents
$N(E)$	distribution of photons with respect to energy (s^{-1} m^{-2} eV^{-1})
N_{tot}	total number of incidents
NHE	normal hydrogen electrode
n	concentration of electrons (cm^{-3})
OH^-	hydroxyl ion
PC	polycrystalline specimen
PEC	photo-electrochemical cell
p	concentration of electron holes (cm^{-3})
pH	$-\log [H^+]$
R	Universal gas constant (8.3144 J $mol^{-1}K^{-1}$)
R	resistance (Ω)
$R(H_2)$	rate of hydrogen generation (mol s^{-1})
S	surface area (m^2)
SC	single crystal
TF	thin film
t	time
U_a	anodic over-potential (V)
U_c	cathodic over-potential (V)
U_{fb}	flat band potential (V)
V_{bias}	bias voltage (V)
V_B	surface potential (corresponding to band curvature) (V)
$V_{n,d}$	cathodic decomposition potential (V)
$V_{p,d}$	anodic decomposition potential (V)
V_H	potential drop across the Helmholtz layer (V)
V_h	potential drop across the hybrid photo-electrode (V)
$V_{ph}(Si)$	photo-voltage across the Si cell (V)
V_{ph} (TiO_2)	photo-voltage across the oxide photo-electrode (V)
x	number (related to nonstoichiometry in chemical formulas)
X	anion in salts, such as Cl^- or SO_4^{2-}
z	number of electrons (electron holes)
$[H^+]$	concentration of hydrogen ions (M)
Δ	difference
σ	electrical conductivity (Ω^{-1} cm^{-1})
μ_i	mobility of ionic charge carriers (cm^2 V^{-1} s^{-1})

μ_n	mobility of electrons ($cm^2\ V^{-1}\ s^{-1}$)	λ_i	threshold wavelength
μ_p	mobility of electron holes ($cm^2\ V^{-1}\ s^{-1}$)	v	frequency (Hz)
η_g	fraction of efficient solar irradiance	α	angle (rad)
η_{ch}	chemical efficiency of irradiation	ϕ	work function (eV)
η_{QE}	quantum efficiency	ϕ_a	work function of photo-anode (eV)
λ	wavelength (nm)	ϕ_{el}	work function of electrolyte (eV)

how close is the hydrogen age. The diagram in Fig. 1 shows that, while the introduction of fuel cell technology will lead to a substantial reduction in the emissions of greenhouse gases (expressed in carbon units per kilometer), the use of fuel cells powered by hydrogen obtained from solar energy will reduce the emissions to nearly zero [5]. Hydrogen is not present in nature in a gaseous form. However, it is abundantly available in plants as well as in several compounds, such as methane, methanol, and higher hydrocarbons. Most importantly, it is available in water. Therefore, hydrogen must be extracted from these compounds.

So far, hydrogen has been produced principally from methane using steam reforming [1,6]. However, this technology results in the emission of CO_2. Also, the hydrogen obtained by water electrolysis using the electricity obtained from the combustion of fossil fuels cannot be considered to be environmentally friendly for the same reason. On the other hand, the use of photo-electricity is considered to be the safe option for hydrogen generation. Further, such hydrogen represents a storable fuel that is produced from a nonstorable source of energy (photo-electricity).

1.2. Hydrogen generation using solar energy

The general enthusiasm for the use of hydrogen as an environmentally friendly fuel has been encouraged by the fact that the combustion of hydrogen results in the generation of water, which neither results in air pollution nor leads to the emission of greenhouse gases. This consideration is correct—assuming that hydrogen is generated using a source of renewable energy, such as solar, wind, hydro-electric, or hydrothermal energy. To date, the technologies for hydrogen generation using sources of renewable energy are in the incubation stage. The growing interest in hydrogen has resulted from the increasing need to develop hydrogen technologies that are based on the utilization of renewable sources of energy. The countries having access to such technologies are likely to form the OPEC of the near-future. Therefore, the development of hydrogen generation technologies based on sources of renewable energy is expected to demand substantial support from both government programs and major energy producers.

There is a large body of literature that indicates that the most promising method of hydrogen generation using a source of renewable energy is that based on photo-electrochemical water decomposition using solar energy [7–51]. Since the first reports of this method published by Honda et al. [7–10] almost 30 years ago, there have been many papers published on the impact of different structures and materials on the performance of photo-electrochemical cells (PECs).

The energy conversion efficiency of water photo-electrolysis is determined principally by the properties of the materials used for photo-electrodes. Consequently, commercial applications for hydrogen generation from solar energy and water will be determined by the progress in materials science and engineering applied to the candidate materials for photo-electrodes.

1.3. Materials aspects of photo-electrochemical cells (PECs)

The materials required for the photo-electrodes of PECs should perform two fundamental functions:

- optical function required to obtain maximal absorption of solar energy;
- catalytic function required for water decomposition.

Most PEC photo-electrodes that exhibit sustainable performance are fabricated from oxide materials [7–34,36,39–51], although the application of valence semiconductors, such as GaAs, has been studied as well [52,53]. The properties of photo-electrodes should satisfy several specific requirements in terms of semiconducting and electrochemical properties, including [10,22,27,38,51]:

- band gap
- flat band potential
- Schottky barrier
- electrical resistance
- Helmholtz potential
- corrosion resistance
- Microstructure

Consequently, the development of high-efficiency photo-electrodes that satisfy all of these requirements entails

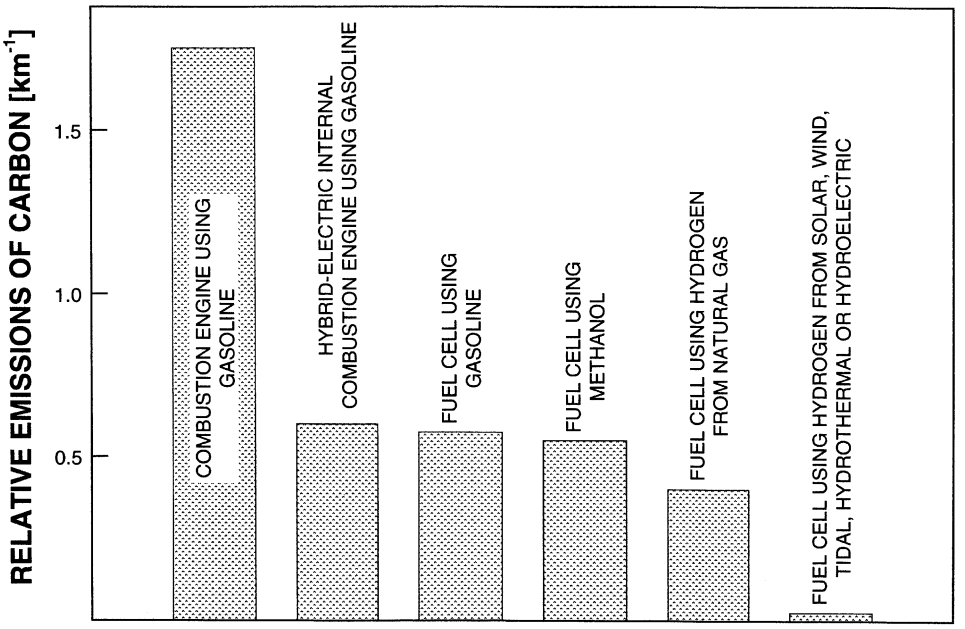

Fig. 1. Relative emission of greenhouse gases (expressed in carbon units per km) for vehicles powered by today's internal combustion engine using gasoline compared to vehicles powered by fuel cells [5].

processing of the materials in order to achieve optimized properties in terms of performance characteristics, including:

- high efficiency
- durability
- low cost of manufacturing
- low cost and ease of maintenance

These properties and performance characteristics will be achieved principally through the imposition of bulk vs. interface properties in a controlled manner. This challenging requirement can be met through the development of new processing technologies that address this issue and characterization techniques that allow the determination of the electrochemical properties of interfaces.

It has been documented that interfaces have a substantial impact on functional properties. For example, grain boundaries may act as weak links for the charge transport in polycrystalline materials [54–57]. On the other hand, these grain boundaries also may act as recombination traps for electronic charge carriers [22,51].

The science and engineering of materials interfaces is an area in which a substantial progress has been made recently. This progress is due to the development of new experimental approaches in the studies of surface properties of compounds [54] and, particularly, in situ monitoring of surface properties during materials processing [55]. The latter techniques allow the processing of materials with controlled surface properties that exhibit targeted functionalities in electrochemical devices.

The purpose of the present work is to consider the progress in R& D on PECs for hydrogen generation from water using solar energy. Specifically, the work considers the key materials properties of photo-electrodes and the trends in research aiming at the development of photo-electrodes that may bring the PEC technology to commercial maturity. Finally, the economic aspects of the use of hydrogen as a fuel are outlined. These considerations are limited solely to oxide materials, which appear to exhibit superior properties as photo-electrodes in comparison to other types of materials.

2. Photo-electrochemistry of water decomposition

2.1. Principles

In the most simple terms, the principle of photo-electrochemical water decomposition is based on the conversion of light energy into electricity within a cell involving two electrodes, immersed in an aqueous electrolyte, of which at least one is made of a semiconductor exposed to light and able to absorb the light. This electricity is then used for water electrolysis. In theory, there are three options for the arrangement of photo-electrodes in the assembly of

PECs [10,22,51,58,59].

- photo-anode made of n-type semiconductor and cathode made of metal;
- photo-anode made of n-type semiconductor and photo-cathode made of p-type semiconductor;
- photo-cathode made of p-type semiconductor and anode made of metal.

The following sections will be limited to the first photo-cell option, although the performance principles of PECs are the same for all three options.

2.2. Reaction mechanism

Water photo-electrolysis using a PEC involves several processes within photo-electrodes and at the photo-electrode/electrolyte interface, including:

- light-induced intrinsic ionization of the semiconducting material (the photo-anode), resulting in the formation of electronic charge carriers (quasi-free electrons and electron holes);
- oxidation of water at the photo-anode by electron holes;
- transport of H^+ ions from the photo-anode to the cathode through the electrolyte and transport of electrons from photo-anode to the cathode through the external circuit;
- reduction of hydrogen ions at the cathode by electrons.

Light results in intrinsic ionization of n-type semiconducting materials over the band gap, leading to the formation of electrons in the conduction band and electron holes in the valence band:

$$2hv \rightarrow 2e' + 2h^{\bullet}, \quad (1)$$

where h is the Planck's constant, v the frequency, e' the electron, $h^{\bullet}$ the electron hole.

Reaction (1) may take place when the energy of photons (hv) is equal to or larger than the band gap. An electric field at the electrode/electrolyte interface is required in order to avoid recombination of these charge carriers. This may be achieved through modification of the potential at the electrode/electrolyte interface.

The light-induced electron holes result in the splitting of water molecules into gaseous oxygen and hydrogen ions:

$$2h^{\bullet} + H_2O_{(liquid)} \rightarrow \frac{1}{2}O_{2(gas)} + 2H^+. \quad (2)$$

This process takes place at the photo-anode/electrolyte interface. Gaseous oxygen evolves at the photo-anode and the hydrogen ions migrate to the cathode through the internal circuit (aqueous electrolyte). Simultaneously, the electrons, generated as a result of Reaction (1) at the photo-anode, are transferred over the external circuit to the cathode, resulting in the reduction of hydrogen ions into gaseous hydrogen:

$$2H^+ + 2e' \rightarrow H_{2(gas)}. \quad (3)$$

Accordingly, the overall reaction of the PEC may be expressed in the form:

$$2hv + H_2O_{(liquid)} \rightarrow \frac{1}{2}O_{2(gas)} + H_{2(gas)}. \quad (4)$$

Reaction (4) takes place when the energy of the photons absorbed by the photo-anode are equal to or larger than E_t, the threshold energy:

$$E_i = \frac{\Delta G^0_{(H_2O)}}{2N_A}, \quad (5)$$

where $\Delta G^0_{(H_2O)}$ is the standard free enthalpy per mole of Reaction (4) = 237.141 kJ/mol; N_A = Avogadro's number = 6.022×10^{23} mol^{-1}.

This yields:

$$E_i = hv = 1.23 \text{ eV} \quad (6)$$

According to Eq. (6), the electrochemical decomposition of water is possible when the electromotive force of the cell (EMF) is equal to or larger than 1.23 V.

The most frequently studied material for the photo-anode is TiO_2 [7–14,17,20–24,26–35,37–41, 43–51]. Despite its high band gap of 3 eV, it is the favored material owing to its high corrosion resistance. The maximal value obtained for the photo-voltage of a PEC equipped with a photo-anode of TiO_2 is $\sim$ 0.7–0.9 V [12]. Consequently, at present, the application of this material as a photo-electrode requires a bias in order to decompose water through one of the following procedures:

- imposition of an external bias voltage;
- imposition of an internal bias voltage through the use of different concentrations of hydrogen ions;
- imposition of an internal bias voltage through the use of a photovoltaic unit in conjunction with the photo-anode (hybrid electrode [17]).

A photo-electrochemical cell for the photo-electrolysis of water and the associated electrochemical chain are shown in Figs. 2 and 3, respectively. A typical cell involves both a photo-anode (made of an oxide material) and cathode (made of Pt) immersed in an aqueous solution of a salt (electrolyte). The process results in oxygen and hydrogen evolution at the photo-anode and cathode, respectively. The related charge transport involves the migration of hydrogen ions in the electrolyte and the transport of electrons in the external circuit.

2.3. Photo-catalytic water decomposition

Concerning the mechanisms of the reactions, the principle of photo-catalytic water decomposition is similar to that of photo-electrochemical water decomposition [60,61]. The essential difference between the two consists of the location of the sites of Reactions (2) and (3). In the photo-electrochemical process, these reactions take place at the photo-anode and cathode, respectively. In the

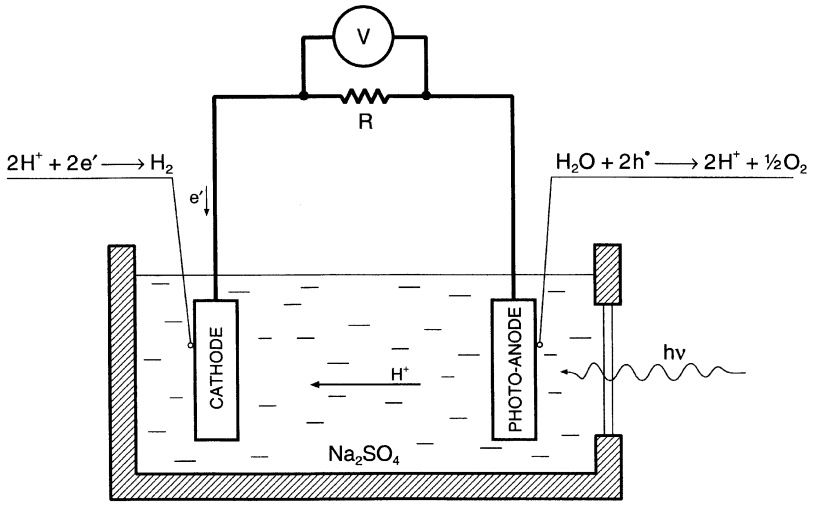

Fig. 2. Structure of photo-electrochemical cell (PEC) for water photo-electrolysis [7].

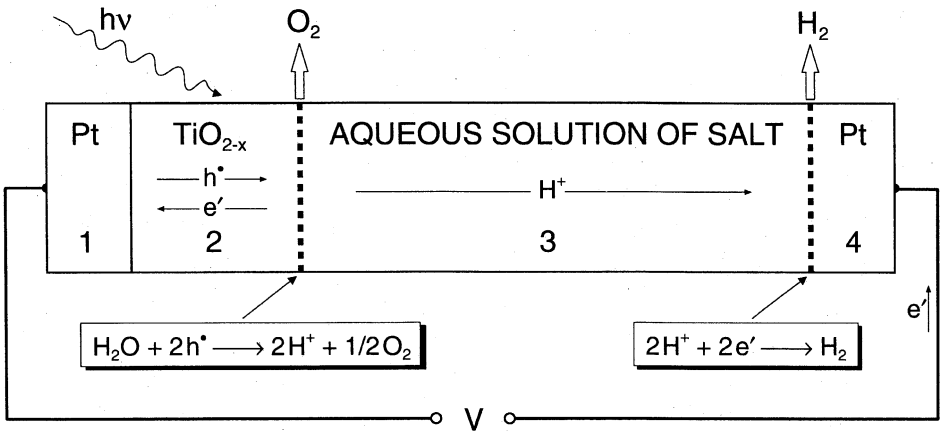

Fig. 3. Electrochemical chain of PEC cell shown in Fig. 2.

photo-catalytic process, both oxidation and reduction occur on the surface of the photo-catalyst, which exhibits the functions of both anode and cathode. The practical difference between photo-catalytic and photo-electrochemical water decomposition is that the latter results in both oxygen and hydrogen evolving separately while, in the former, a mixture of both gases is evolved.

3. Formation of electrochemical chain of PEC (band model representation)

The band structures of both electrodes, involving the photo-anode of an n-type semiconductor and metallic cathode, at different stages in the formation of the electrochemical chain of the PEC, are shown schematically in Figs. 4–7. These figures show the band structure, illustrating various energy quantities, such as work function; band levels of the electrodes before and after the chain is established (in comparison with the potentials corresponding to the H^+/H_2 and O_2/H_2O redox couples); and band bending. Fig. 4 shows the energy diagram before the galvanic contact is made between the two electrodes. As seen in Fig. 5, the contact between the two electrodes (in the absence of light) results in electronic charge transfer from the solid of lower work function (semiconductor) to the solid of higher work function (metal) until the work functions of both electrodes assume the same value. This charge transfer results in a change in the semiconductor surface's electrical potential by V_B, leading to band bending. This energy relation is not favourable for water decomposition because the H^+/H_2 energy level is above the Fermi energy level of the cathode.

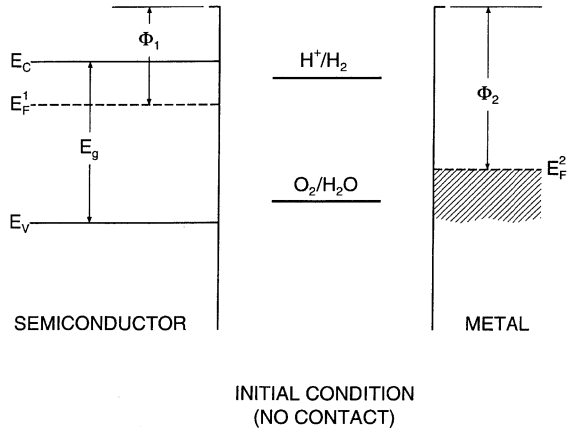

Fig. 4. Energy diagram of PEC components: anode (semiconductor), electrolyte, and cathode (metal) before galvanic contact.

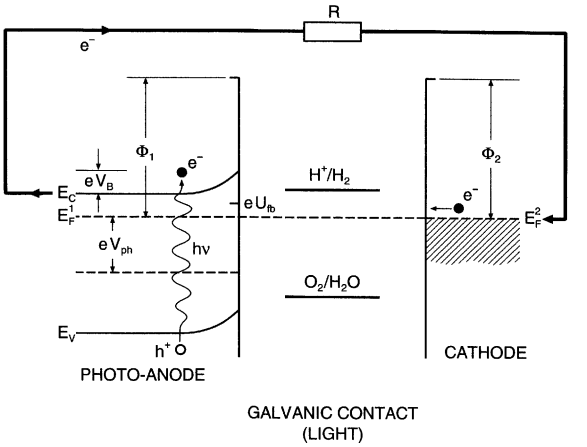

Fig. 6. Effect of light on electronic structure of PEC components.

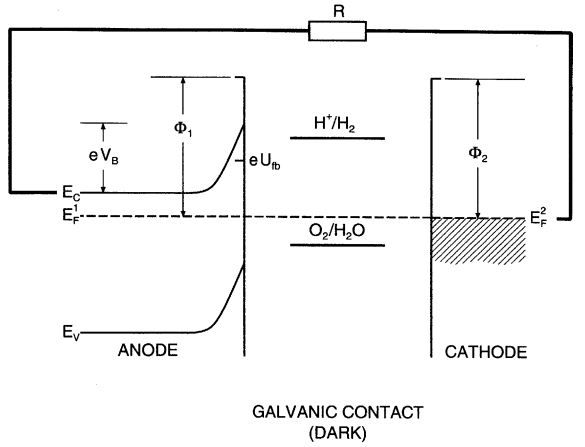

Fig. 5. Energy diagram of PEC components after galvanic contact between anode and cathode.

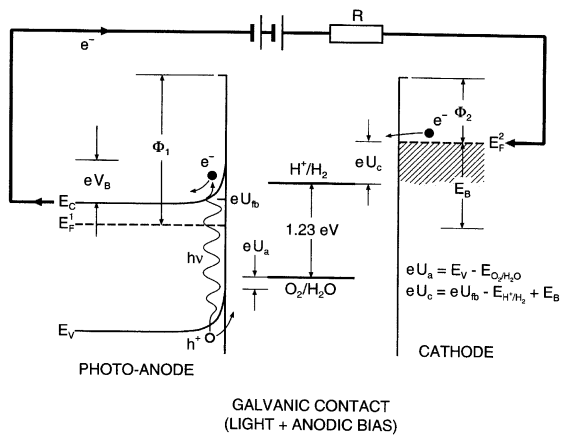

Fig. 7. Effect of light on energy diagram of PEC with externally applied bias.

As seen in Fig. 6, the application of light results in the lowering of the surface potential of the photo-anode and the lowering of the H^+/H_2 potential. However, the latter still is above the E_F level of the cathode. Consequently, Fig. 7 shows that the application of an anodic bias is required to elevate the cathode E_F level above the H^+/H_2 energy level, thus making the process of water decomposition possible.

4. Impact of band structure of photo-electrode material on solar energy conversion efficiency

4.1. Solar energy spectrum

The purpose of the present section is to consider the impact of the semiconducting properties of the photo-electrode on the solar energy conversion efficiency in photo-electrolysis. Fig. 8 schematically illustrates the solar spectrum in terms of the number of photons vs. the photon energy. The shaded area below the spectrum curve corresponds to the flux of photons (J) of energy equal to or larger than E_i:

$$J = \int_{E_i}^{\infty} N(E)\,\mathrm{d}E \quad [\mathrm{s}^{-1}\,\mathrm{m}^{-2}], \tag{7}$$

where $N(E)$ is the distribution of photons with respect to their energy, E the energy of photons, E_i the threshold energy.

The band gap of the photo-electrode has a critical impact on the energy conversion of photons [62,63]. That is, only the photons of energy equal to or larger than that of the band gap may be absorbed and used for conversion. The maximal conversion efficiency of photovoltaic devices may be achieved at band gaps in the range 1.0–1.4 eV; this will be discussed subsequently in Section 8.2.3.

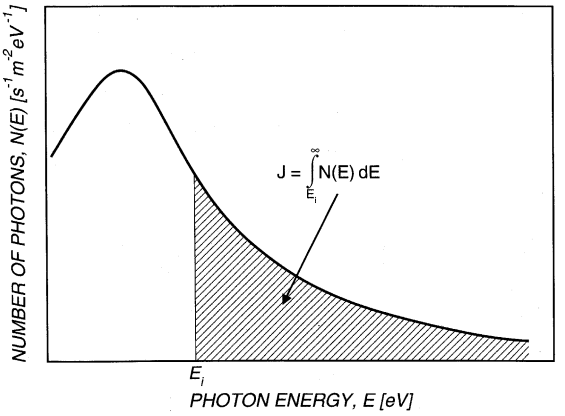

Fig. 8. Schematic illustration of light spectrum (number of photons vs. photon energy), showing photon flux available for conversion at energy $\geqslant$ energy E_i.

Fig. 9 illustrates the solar energy spectrum, depicting segments defining phonon fluxes corresponding to different energy ranges. Theoretically, the lowest limit for the band gap of a PEC's photo-anode is determined by the energy required to split the water molecule (1.23 eV), which is determined by the photon flux as represented by the integral of $J_1 - J_2$. Accordingly, this photon flux, within this part of the spectrum, is not available for conversion owing to the theoretical energy limit of 1.23 eV [62].

In practice, the energy that may be used for conversion is smaller than the theoretical energy limit. The difference between the two is due to energy losses caused by the following [63]:

- polarization within the PEC;
- recombination of the photo-excited electron–hole pairs;
- resistance of the electrodes;
- resistance of the electrical connections;
- voltage losses at the contacts.

The estimated value of these combined losses is $\sim$ 0.8 eV ($J_2 - J_3$); this part of the spectrum is not available for conversion. Therefore, the optimal energy range in terms of the photons available for conversion is $\sim$ 2 eV. This situation is represented in Fig. 9 by the integral of $J_1 - J_3$.

In consequence, the energy corresponding to the photon flux J_3 in Fig. 9 is available for conversion. However, the availability of this energy is contingent upon the use of a photo-anode with band gap of 2 eV. Unfortunately, oxide semiconductors that have such a band gap, such as Fe_2O_3, are susceptible to corrosion, as will be discussed subsequently in Section 5.6.

The material that has been used most frequently as a photo-anode, due to its high corrosion resistance, is TiO_2. However, its band gap is 3 eV [7,10,14,17] and, consequently, the part of the energy spectrum available for conversion corresponds to photon flux J_4. Thus, there is a need to increase the amount of energy available for conversion from J_4 to J_3. This can be done by processing a corrosion-resistant material, which is the challenge for materials engineers.

Alternatively, the solar energy spectrum frequently is considered in terms of radiation energy vs. wavelength, as shown in Fig. 10. The area under this spectrum is termed incidence of solar irradiance, I_r. The effectiveness of the conversion is determined by the part of the spectrum over which the photons exhibit energies equal to or higher than that available for conversion, λ_i, which is shown in Fig. 11:

$$I_r = \int_0^{\lambda_i} E(\lambda)\,\mathrm{d}\lambda \quad [\mathrm{W\,m^{-2}}]. \tag{8}$$

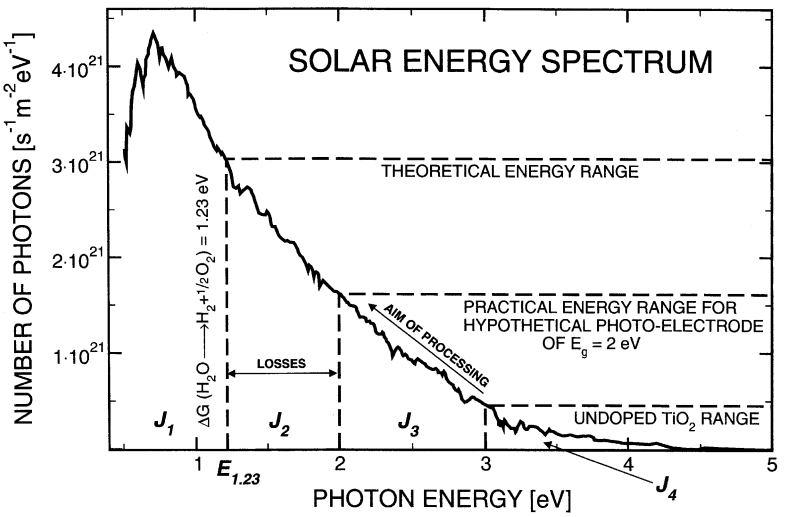

Fig. 9. Solar energy spectrum (AM of 1.5) in terms of number of photons vs. photon energy, showing different flux photon regimes corresponding to specific properties of photo-electrodes [62].

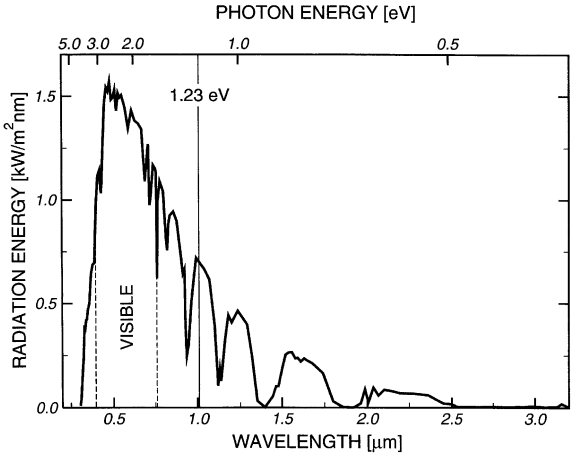

Fig. 10. Solar energy spectrum (AM of 1.5) in terms of radiation energy vs. photon wavelength [63].

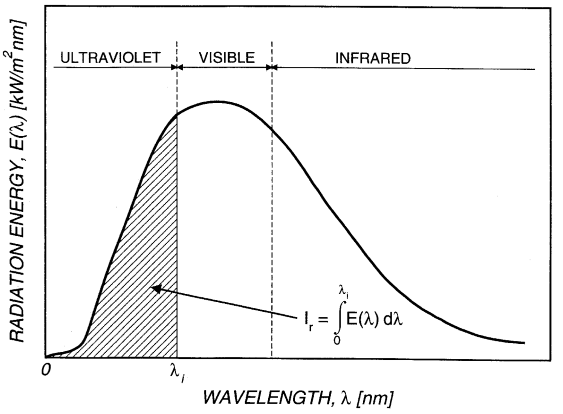

Fig. 11. Schematic illustration of light spectrum (radiation energy vs. wavelength), showing incidence of solar irradiance (I_r) available for conversion.

4.2. Radiation standard

The effect of the earth's atmosphere on solar radiation is considered in terms of the so-called *air mass* (AM):

$$\mathrm{AM} = \frac{1}{\cos\alpha}, \tag{9}$$

where α is the angle between the overhead and actual position of the sun.

At the Earth's surface, the AM assumes values between unity ($\alpha = 0$) and infinity ($\alpha = 90^\circ$). The AM characterizes the effect of the Earth atmosphere on solar radiation and, therefore, depends on geographical position, local time, and date. It is assumed that, outside the Earth's atmosphere, the AM is zero. The radiation standard [63] assumes an AM of 1.5, which corresponds to $\alpha = 0.841$ radians or 48°. Of course, the solar energy available for conversion depends also on local atmospheric conditions, such as cloudiness, air pollution, airborne dust particles, and relative humidity.

4.3. Property limitations of oxide materials as photo-electrodes

Fig. 12 shows that the band gaps of candidate oxide materials for photo-electrodes vary between 2.3 and 3.7 eV.

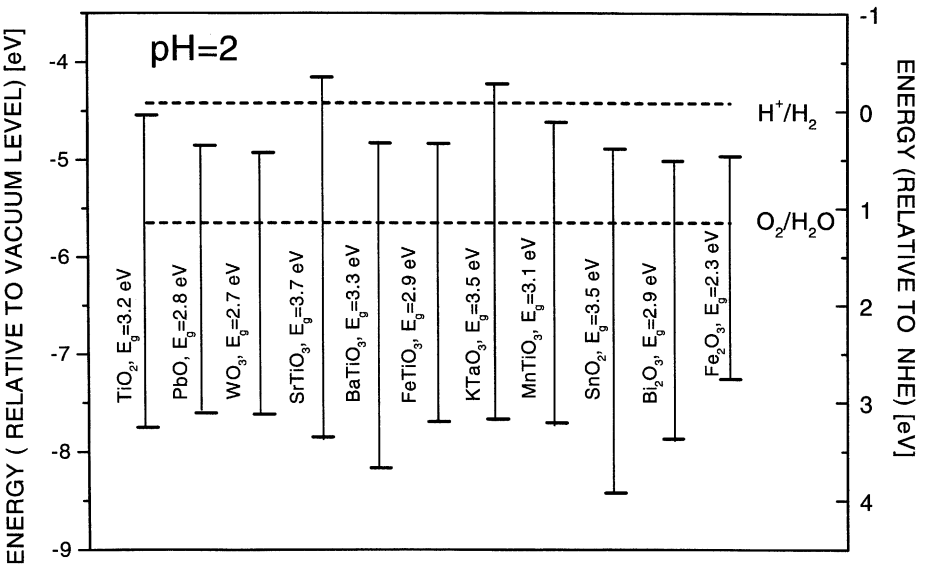

Fig. 12. Diagram showing band gap energy of different oxide materials and relative energies with respect in terms of vacuum level and normal hydrogen electrode level in electrolyte of pH = 2 [64].

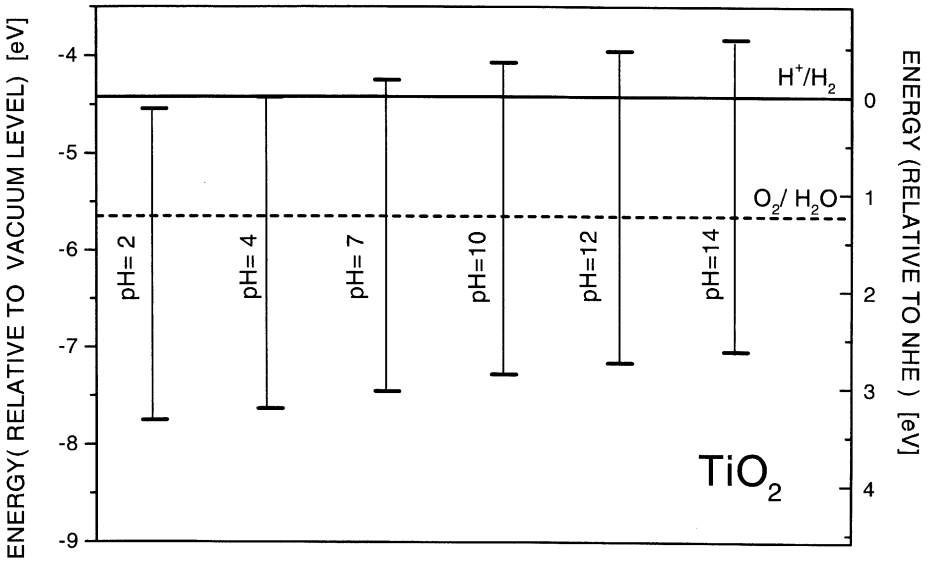

Fig. 13. Effect of pH on energy of TiO_2 in terms of vacuum level and normal hydrogen electrode level in electrolyte.

These data are shown in terms of their energies compared to the vacuum level and the normal hydrogen electrode (NHE) level in an aqueous solution of pH = 2 [64]. Unfortunately, the most promising materials from the viewpoint of the band gap width, such as Fe_2O_3 ($E_g = 2.3$ eV) [65], GaP ($E_g = 2.23$ eV) [66], and GaAs ($E_g = 1.4$ eV) [66], are not stable in aqueous environments and so exhibit significant corrosion by water. Therefore, these materials are not suitable as photo-electrodes in aqueous environments. The most promising oxide materials, which are corrosion resistant, include TiO_2 and $SrTiO_3$ [7–14,17, 20–35, 37–51].

Fig. 13 shows the effect of pH on the energy bands of TiO_2 vs. the vacuum level and the normal hydrogen electrode (NHE) level in aqueous solutions. These data show that adjustment of the pH to the lowest levels results in moving the H^+/H_2 potential to the level at which the photo-anode may perform spontaneously.

In some candidate materials, such as In_2O_3, with $E_g =$ 2.6 eV, indirect intrinsic ionization requires higher energies than the band gaps [67]. Therefore, these materials also are not suitable for photo-anodes.

5. Key functional properties of photo-electrodes

The materials used for photo-electrodes satisfy several specific functional requirements with respect to semiconducting and electrochemical properties. Although these properties have been identified, it is difficult to process materials such that all requirements are satisfied. The purpose of the present section is to consider the most important property requirements.

5.1. Band gap

The band gap, E_g, is the smallest energy difference between the top of the valence band and the bottom of the conduction band (see Figs. 4–7). The width between the bands, through which the photon-induced ionization takes place, is an important quantity for materials that are candidates for photo-electrodes.

As discussed in Section 4.1, the optimal band gap for high-performance photo-electrodes is ~ 2 eV [10,22,27,51,58,59]. Such a material, which satisfies this requirement and is corrosion resistant, is not available commercially. Therefore, there is a need to process such a material. One possibility by which this can be achieved is through the imposition of a band located ~ 2 eV below the conduction band. Experimentally, this impurity band can be achieved through the heavy doping of TiO_2 with aliovalent ions. As seen in Fig. 14 [68,69], the most promising dopant to use is $V^{4+/5+}$, which forms the solid solution $(Ti_{1-x}V_x)O_2$ [47,48,70]. However, these reports are not in agreement concerning the effect of doping on the electrochemical properties of TiO_2. Philips et al. [70] have observed that, although the addition of 30 mol% V to TiO_2 results in a reduction in the band gap to 1.99 eV, the formation of $(Ti_{0.7}V_{0.3})O_2$ had a detrimental effect on the photo-activity due to a substantial increase in the flat band potential by $\sim$ 1 V). As a result, this necessitated the imposition of an adequate external bias voltage. On the other hand, Zhao et al. [47,48] observed that increasing the V content resulted in an increase in the energy conversion efficiency. While Philips et al. [70] reported data for single crystals and polycrystalline specimens and Zhao et al. [47,48] studied thin films, it is possible that the effect of V on the

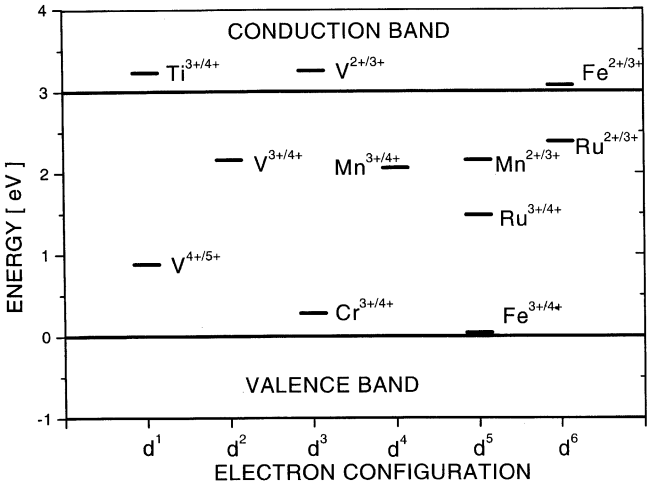

Fig. 14. Energy levels of aliovalent ions in TiO_2 (rutile) lattice [68,69].

photo-electrode is morphological rather than compositional. Further studies in this area are required.

Effective processing of a material with the desired semiconducting properties obtained through doping requires in situ evaluation of the establishment and progression of these properties during processing. This may be achieved by combined measurements of electrical conductivity, thermoelectric power, and work function at elevated temperatures and under controlled gas phase composition [71,72].

Another method of increasing the conversion efficiency is to fabricate a hybrid photo-electrode involving a stack of materials of different band gaps, where each of these absorbs light of different wavelength. The best material that can be exposed to aqueous solutions is TiO_2, which has a limited ability for light absorption due to its high band gap. However, a material with a much lower band gap, such as Si, can be used in the lower part of the stack. In this case, the total amount of energy absorbed would be substantially higher than that of TiO_2 alone. The first such hybrid electrode was reported by Morisaki et al. [17]; this will be discussed subsequently in Section 6.

5.2. Flat-band potential

The flat-band potential, U_{fb}, is the potential that has to be imposed over the electrode/electrolyte interface in order to make the bands flat [22,51,58]. This potential is an important quantity in photo-electrode reactions. Specifically, the process of water photo-electrolysis may take place when the flat-band potential is higher than the redox potential of the H^+/H_2 couple [22,51,58]. The flat-band potential may be modified to the desired level through surface chemistry [48,49].

Fig. 15 shows the flat-band potential of several oxide materials vs. the band gap compared to the vacuum level and the normal hydrogen electrode (NHE) [64]. According to Figs. 6 and 7, photo-cells equipped with a photo-anode made of materials with negative flat-band potentials (relative to the redox potential of the H^+/H_2 couple, which depends on the pH) can split the water molecule without the imposition of a bias. Alternatively, all other materials require a bias in order to generate the total voltage sufficient for water decomposition.

5.3. Schottky barrier

A potential drop in the potential within the interface layer of the solid, formed as a result of concentration gradients, surface states, and adsorption states, is termed a *Schottky barrier*. The Schottky barrier plays an important role in preventing recombination of the charge formed as a result of photo-ionization.

It has been documented that an electrical potential barrier across the surface layer can be formed as a result of the following [47–49]:

- structural deformations within the near-surface layer due to an excess of surface energy;
- segregation-induced chemical potential gradients of aliovalent ions across the surface layer imposed during processing;
- chemical potential gradients of aliovalent ions across the surface layer imposed as a result of surface processing.

Accordingly, the formation of these gradients may be used for the modification of the Schottky barrier in a controlled manner. The use of this procedure requires in situ monitoring of the surface vs. bulk electrochemical properties during the processing of the electrode materials [72].

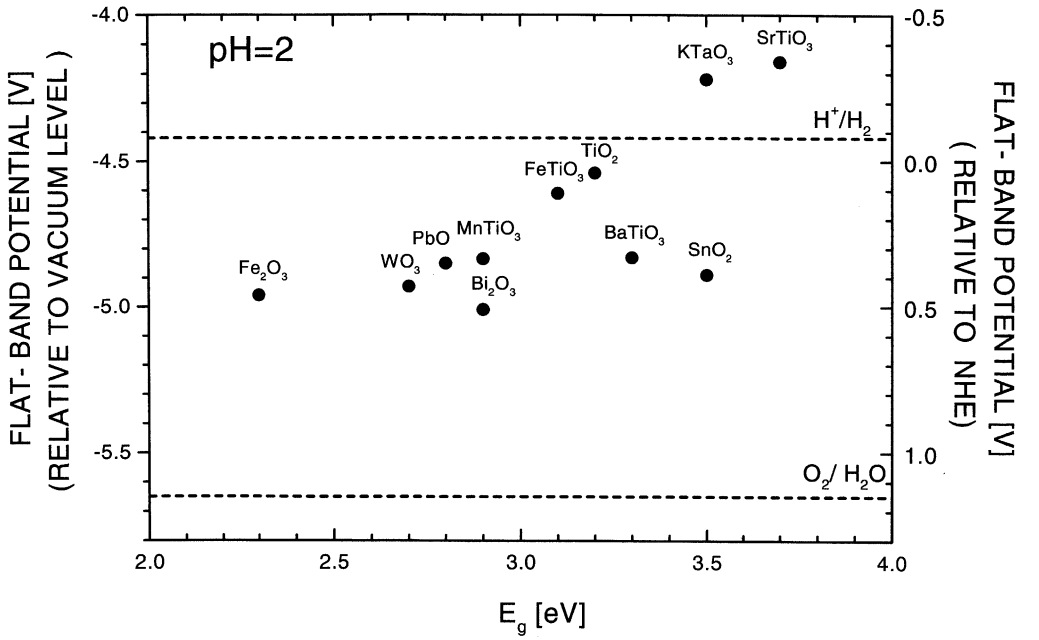

Fig. 15. Flat band potential of different oxide semiconductors vs. energy gap and normal hydrogen energy level in electrolyte of pH = 2 [64].

Studies on the effect of doping on the surface vs. bulk semiconducting properties are needed in order to impose the desired band curvatures. The effect of doping may be assessed through the determination of surface vs. bulk sensitive properties, which can be assessed by work function [55,72] and thermoelectric power (Seebeck coefficient), respectively [71,72].

5.4. Electrical resistance

The major sources of energy losses derive from the ohmic resistances of the external and internal circuits of the PEC, including:

- electrodes
- electrolyte
- electrical leads (wires)
- electrical connections
- measuring and control equipment

In order to achieve the maximum conversion efficiency, the electrical resistances of all of these items must be minimized.

5.4.1. Electrodes

The electrical resistance of the semiconducting photo-anode is several orders of magnitude larger than that of the metallic cathode. The electrical conductivity of the photo-anode, which is determined by the concentration of the charge carriers and their mobilities, is described in Eq. (10):

$$\sigma = en\mu_n + e\,p\mu_p + Z_i ei\mu_i, \tag{10}$$

where n is the concentration of electrons, p the concentration of electron holes, i the concentration of ions, μ_n the mobility of electrons, μ_p the mobility of electron holes, μ_i the mobility of ion, Z_i charge number of ion.

At room temperature, the ionic component of the electrical conductivity may be ignored. The mobility terms do not change with concentration when interactions between the charge carriers are absent. However, at higher concentrations, these interactions result in a decrease in the mobilities. Therefore, the maximal σ is a compromise between the effect of increasing the concentrations while decreasing the mobilities. The optimal value of σ may be achieved through the imposition of a defect disorder that is optimal for conduction [72]. The defect disorder and electrical properties may be modified through the incorporation of aliovalent cations (forming donors and acceptors) and the imposition of controlled oxygen partial pressure during processing. Again, these required electrical properties may be achieved through in situ monitoring of the electrical conductivity, thermo- electric power, and work function during processing [71,72].

The electrical resistance of the TiO_2 photo-electrode may be reduced by partial reduction of TiO_2 at high temperatures in a hydrogen/argon mixture. In nonstoichiometric TiO_{2-x}, the higher x, the lower the resistance [71,72]. It would be expected that the resistance of the photo-anode during performance of a PEC in contact with oxygen would increase due

to oxidation. Therefore, the electrical resistance of PEC's must be regenerated after oxidation by postreduction in a hydrogen/argon mixture.

An alternative method of reducing the resistance is through minimization of the thickness of the photo-electrode by fabrication of a thin film. This method has the advantage that the substrate can be made of Ti metal, which imposes a strong reduction potential, thereby possibly obviating the need for post-reduction.

5.4.2. Electrolyte

Analogous to the situation concerning the semiconducting electrode, maximal conduction of the electrolyte may be achieved by selection of optimal ions and their concentrations, leading to maximal mobility. The ions with the highest mobilities are H^+ and OH^-. However, their use in high concentrations is problematic owing to their chemical aggressiveness. Alkaline cations, such as K^+ and Ba^{2+}, and anions, such as Cl^- and NO_3^-, are alternative candidates owing to their relatively high mobilities. These ions assume minimal resistances at concentrations between 3 and 4 M.

5.4.3. Electrical leads

Electrical leads usually are made of metal wires with resistances substantially lower than those of the photo-electrode and the electrolyte. In this sense, selection of the wire is of secondary importance.

5.4.4. Electrical connections

Connections, such as those between wires and those between wires and electrodes, may be sources of high resistance due to (i) contact potential difference (CPD), which develops between solids of different work function, and (ii) local corrosion resulting in the formation high-resistance scales. Therefore, it is desirable to minimize or, preferably, eliminate the number of interwire connections. Also, the engineering of other types of connections, those between the leads and the other circuit elements, is of considerable importance.

The issue of the connections is particularly important for the elements of hybrid electrodes, which involve a stack of different semiconducting materials [17]; this will be discussed subsequently in Section 6.

5.4.5. Measuring and control equipment

The internal resistances of the measuring and control equipment are important because it is essential to maintain these resistances at the appropriate levels. That is, voltmeters should have resistances as high as possible and ammeters should have resistances as low as possible.

5.5. Helmholtz potential barrier

When a semiconducting photo-electrode material is immersed in a liquid electrolyte (in which the chemical potential of the electrons is determined by the H^+/H_2 redox potential), the charge transfer at the solid/liquid interface results in charging of the surface layer of the semiconductor. The charge transfer from the semiconductor to the electrolyte leads to the formation of a surface charge and results in upwards band bending, forming a potential barrier, as shown in Fig. 16. This barrier is similar to that of the solid/solid interface, shown in Fig. 5. This surface charge is compensated by a charge of the opposite sign, which is induced in the electrolyte within a localized layer, known as the *Helmholtz layer*. It is $\sim$ 1 nm thick and is formed of oriented water molecule dipoles and electrolyte ions adsorbed at the electrode surface [51,73,74]. The height of this potential barrier, known as the *Helmholtz barrier*, is determined by the nature of the aqueous environment of the electrolyte and the properties of the photo-electrode surface.

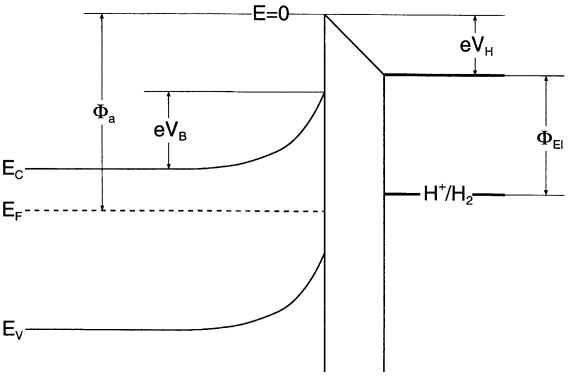

Fig. 16. Energy diagram of solid/liquid interface consisting of photo-anode (n-type semiconductor) and electrolyte.

The performance characteristics of PECs depend, to a large extent, on the height of the Helmholtz barrier [51]. Therefore, it is essential to obtain further information on (i) the effect of the specific properties of the electrode/electrolyte interface on the height of the barrier and (ii) the determination of the effect of the Helmholtz barrier on the efficiency of the photo-electrochemical process.

5.6. Corrosion and photo-corrosion resistance

An essential requirement for the photo-electrode is resistance to reactions at the solid/liquid interface, resulting in degradation of its properties. These reactions include:

- electrochemical corrosion
- photo-corrosion
- dissolution

Any form of reactivity results in a change in the chemical composition and the related properties of the electrode and photo-electrode [51,58]. These processes are particularly

damaging to the properties of the photo-electrode, which are essential for photo-conversion. Therefore, is essential for the photo-electrodes to be resistant to these types of undesired reactivities.

Certain oxide materials, such as TiO_2 and its solid solutions, are particularly resistant to these reactivity types [7,17,51]. Therefore, they are suitable candidates for photo-electrodes for electrochemical water decomposition.

A large group of valence semiconductors [52,53], which exhibit suitable semiconducting properties for solar energy conversion (width of band gap and direct transition within the gap), are not resistant to these types of reactivity (see Fig. 17). Consequently, their exposure to aqueous environments during the photo-electrochemical process results in the deterioration of their properties as photo-electrodes mainly due to electrochemical corrosion.

In liquid environments, corrosion is an electrochemical process when it is accompanied by charge transfer at the solid/liquid interface. The electrochemical corrosion of an AB semiconductor, which leads to anodic and cathodic decomposition, may be represented by the following reactions, respectively:

$$AB + zh^{\cdot} \rightarrow A^{+z} + B + \Delta G_a, \tag{11}$$

$$AB + ze' \rightarrow B^{-z} + A + \Delta G_c, \tag{12}$$

where z is the number of electrons or holes, ΔG_a the free energy change at the anode, ΔG_c the free energy change at the cathode.

ΔG_a and ΔG_c are related to the following enthalpy terms at the anode and cathode, respectively:

$$E_{p,d} = \frac{\Delta G_a}{zN_A}, \tag{13}$$

$$E_{n,d} = \frac{\Delta G_c}{zN_A}, \tag{14}$$

where $E_{p,d}$ is the free enthalpy of oxidation Reaction (11) per one electron hole, $E_{n,d}$ the free enthalpy of reduction Reaction (12) per one electron.

The following criteria for stability of photo-electrodes against electrochemical corrosion have been formulated by Gerischer [74] for the photo-anode and photo-cathode, respectively:

$$E(O_2/H_2O) < E_{p,d}, \tag{15}$$

$$E(H^+/H_2) > E_{n,d}, \tag{16}$$

where $E(H^+/H_2)$ is the energy of the redox couple H^+/H_2, $E(O_2/H_2O)$ the energy of the redox couple H_2/H_2O.

Inequalities (15) and (16) correspond to the energy values on the electrochemical scale (relative to the normal hydrogen electrode NHE) shown in Fig. 17. As seen, this shows band gap ranges and energies of the redox couples ($E_{p,d}$, $E_{n,d}$) for a number of ionic and valence semiconductors. It can be seen that the stability condition (15) required for the photo-anode is not met for all valence semiconductors and Cu_2O (viz., the $E_{p,d}$ level is less than the O_2/H_2O level). Therefore, these compounds are thermodynamically unstable in aqueous environments. On the other hand, several oxide semiconductors, such as TiO_2, SnO_2, and WO_3, are resistant to electrochemical corrosion while ZnO is stable only as a photo-cathode (viz., the $E_{n,d}$ levels are greater than the H^+/H_2 level).

From the viewpoint of its energy gap, GaAs should be an excellent candidate material for solar energy conversion ($E_g = 1.4$ eV). Unfortunately, it is not stable in aqueous environments.

The decomposition mechanism of GaAs depends on the pH of the aqueous environment. In neutral and basic solutions, GaAs reacts with water according to the reaction [67]:

$$GaAs + 6H_2O + 6h^{\cdot} \rightarrow Ga(OH)_3 + As(OH)_3 + 6H^+. \tag{17}$$

In acidic solutions, GaAs exhibits either anodic or cathodic corrosion, which may be represented by the following equilibria, respectively:

$$GaAs + 3e' + 3H^+ \rightarrow Ga + AsH_{3(gas)}, \tag{18}$$

$$GaAs + 2H_2O \rightarrow Ga^{+3} + AsO_2^- + 6e' + 4H^+. \tag{19}$$

The products of both reactions, including $As(OH)_3$ and AsH_3, are highly toxic.

Efforts have been made to protect valence semiconductors from corrosion by imposition of protective layers [75–78]. However, this type of protection results in a substantial reduction in the energy conversion efficiency.

5.7. Microstructure

It is anticipated that future commercial photo-electrodes will be polycrystalline rather than single-crystal. So far, little is known of the effect of interfaces, such as surface linear defects caused by grain boundaries, on photo-electrochemical properties of photo-electrodes. Therefore, there is an urgent need for the following:

- Understanding of the effect of the microstructure of polycrystalline photo-electrodes, specifically that of surface structural defects, on the photo-electrochemical properties.
- Development of interface processing technologies leading to the optimization of the energy conversion efficiency of photo-electrodes of polycrystalline materials.

6. Photo-cell structures

The PECs reported in the literature may be categorized as follows:

- single photo-electrode system;
- hybrid photo-electrode [21,74];

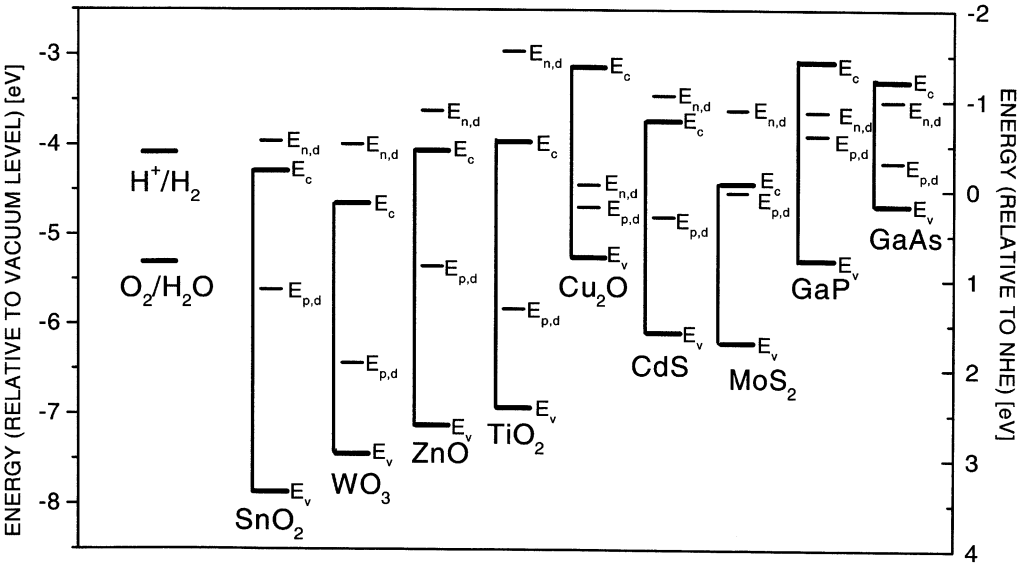

Fig. 17. Position of decomposition potentials $E_{n,d}$ and $E_{p,d}$ vs. E_c and E_v of selected semiconducting materials [74].

- photo-electrode sensitized through doping by foreign ions [30,47,59,79–94,70,95–111];
- photo-electrode sensitized through incorporation of particles of noble metals [39,95,112–116];
- photo-electrode sensitized through dye deposition [117–123];
- bi-photo-electrode system [23].

The single photo-electrode PEC system, similar to that reported by Fujishima and Honda [7], is equipped with one photo-electrode while the second electrode is not light-sensitive.

The bi-photo-electrode system is based on the use of semiconducting materials as both photo-electrodes [23]. In this, case n- and p-type materials are used as the photo-anode and photo-cathode, respectively. The advantage of such system is that the photo-voltages are generated on both electrodes, resulting, in consequence, in the formation of an overall photo-voltage that is sufficient for water decomposition without the application of a bias.

The concept of a hybrid photo-anode is based on the use of two different n-type semiconductors that form a heterogeneous system [74]. However, in this case, the external materials exposed to light must be transparent to radiation.

Both the bi-photo-electrode and hybrid photo-electrode systems allow a substantial increase of solar energy conversion [23]. The quantitative aspects of this are considered in Fig. 9.

Morisaki et al. [17] reported a hybrid photo-electrode (HPE), consisting of a combination PEC made of a TiO_2 layer, forming the photo-anode, and Si photovoltaic cell underneath.

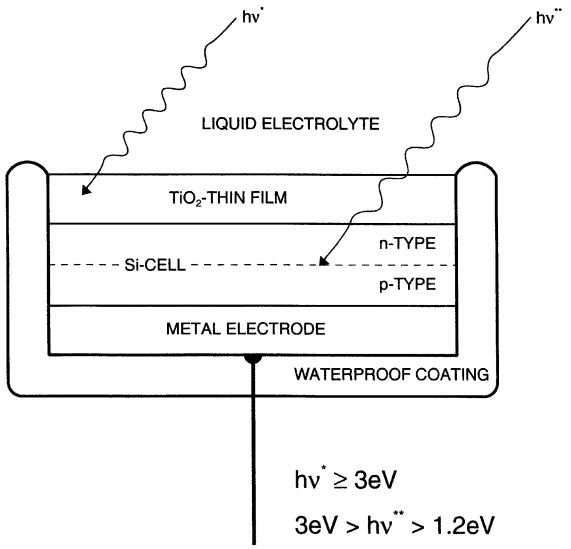

Fig. 18. The hybrid photo-electrode (HPE), involving TiO_2 photo-anode and Si solar cell (according to Morisaki et al. [17]).

Fig. 18 illustrates the structure of the HPE, involving the metal contact, Si photovoltaic cell, photo-anode of TiO_2, and aqueous electrolyte [17]. In this structure, only the TiO_2 layer is exposed to the aqueous environment, while the Si solar cell forms a sublayer that is not in contact with the electrolyte. The purpose of the Si solar cell is to generate a photo-voltage that can be used as an internal electrical bias. Consequently, this type of HPE cell is expected to exhibit intrinsic (spontaneous) performance in the absence

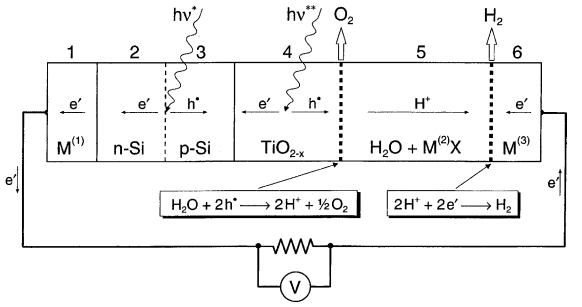

Fig. 19. Electrochemical chain of PEC incorporating HPE shown in Fig. 18.

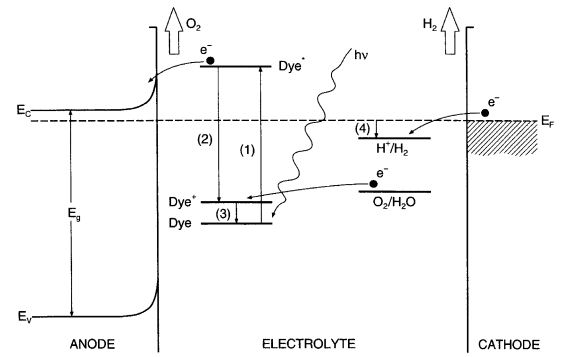

Fig. 20. Principle of performance of PEC involving sensitized photo-anode.

of an external bias. Fig. 19 shows the electrochemical chain incorporated within the HPE.

The HPE cell allows very efficient use of solar energy. Although the external layer of TiO_2 absorbs only photons of energy $\geqslant 3$ eV, the remaining part of the solar spectrum is transmitted to the Si solar cell (beneath the TiO_2 layer), which has $E_g = 1.2$ eV. Consequently, the Si cell absorbs the photons of the energy between 1.2 and 3 eV. According to Morisaki et al. [17], the anodic bias generated by the Si cell is ~ 0.7 V. Since a PEC based solely on TiO_2 exhibits ~ 0.8 V, this gives a total HPE output of ~ 1.5 V, which is sufficient for the efficient performance of an HPE.

The performance of most of PECs reported in the literature requires the imposition of an electrical bias by an external d.c. voltage. Such an external bias may be considered as environmentally friendly only when provided by a source of renewable energy, such as a photovoltaic unit. A bias also may be imposed through the use of electrolytes of two different pH values over the anode and cathode, so producing a chemical bias. This arrangement requires the use of an ionic bridge (e.g., agar) dividing the two electrolytes. The voltage imposed by the chemical bias is determined at room temperature by the pH difference between the two electrolytes:

$$\Delta V = \frac{2.303RT}{F}\Delta p\mathrm{H} = 0.059\Delta p\mathrm{H} \quad [\mathrm{V}], \tag{20}$$

where R is the universal gas constant, T the absolute temperature, F the Faraday constant.

Of course, the chemical bias maintains a constant value as long as an open-circuit voltage (EMF) is measured. The performance of a PEC and the associated photo-current flowing between the electrodes lead to the consumption of OH^- and H^+ ions at the anodic and cathodic cell compartments, respectively. Consequently, this results in the neutralization of the electrolyte and a reduction of the bias.

Photo-anode sensitization through doping by foreign ions has been discussed in Section 5.1.

It has been reported that photo-anodes made of TiO_2 thin films may be sensitized by incorporation of small particles of noble metals, such as Ag and Pt, thus forming a dispersed system involving micron-sized particles [39,95,112–116]. The conversion efficiency may be increased substantially through dye-sensitization of photo-electrodes [117–123]. The principle of the performance of a PEC equipped with a sensitized photo-anode is shown in Fig. 20. The photo-sensitizer, which is an organic dye, is physically attached to the surface of the photo-electrode. Light absorption by the dye leads to the transformation of the dye molecules from the ground-state (Dye) to the excited-state (Dye^*):

$$\mathrm{Dye} + h\nu \rightarrow \mathrm{Dye}^*. \tag{21}$$

The transition from the excited state (Dye^*) to a higher oxidation state (Dye^+) results in the formation of electrons:

$$\mathrm{Dye}^* \rightarrow \mathrm{Dye}^+ + \mathrm{e}'. \tag{22}$$

Consequently, the oxidized dye molecule reacts with water, resulting in the formation of O_2 at the photo-anode:

$$\mathrm{Dye}^+ + \frac{1}{2}\mathrm{H_2O} \rightarrow \mathrm{Dye} + \frac{1}{4}\mathrm{O_2} + \mathrm{H}^+ \tag{23}$$

and H_2 at the cathode:

$$\mathrm{e}' + \mathrm{H}^+ \rightarrow \frac{1}{2}\mathrm{H_2}. \tag{24}$$

The dye-sensitized semiconducting photo-electrode exhibits two functions, these being (i) absorption of light by the dye and (ii) charge transport by the semiconductor.

Dye sensitization may lead to sustainable performance of photo-electrodes only when sensitizers exhibit a stable performance in aqueous solutions.

7. Dynamics of TiO_2-based PEC

Fig. 21 shows the open circuit voltage vs. time for a PEC based on TiO_2 with an electrochemical chain as shown in

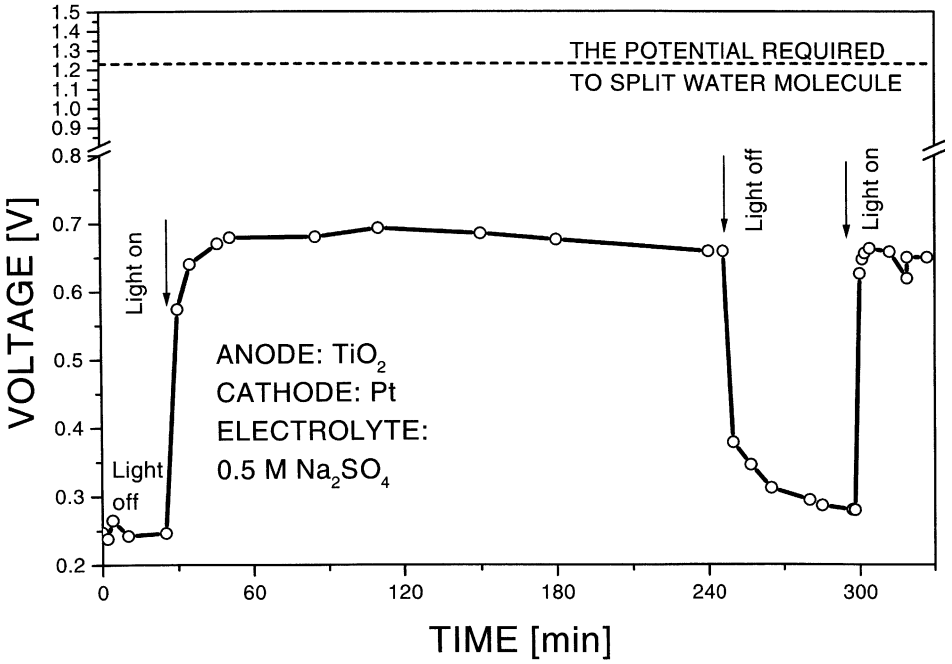

Fig. 21. Dynamics of PEC consisting of TiO_2 thin film as photo-anode, Pt as cathode, and aqueous solution of Na_2SO_4 as electrolyte during light-on and light-off regimes [124].

Fig. 3. This cell involves two electrodes immersed in the same electrolyte [124]. The plot was recorded during a sunny day when the air mass (AM) was near its standard level of 1.5. As seen, the photo-voltage reaches its maximum value within 25 min after exposure to sunlight and the initial value is restored within 1 h after the sun exposure is terminated. The voltage generated in this cell (EMF = 0.7 V) is less than that required for water decomposition because the U_{fb} level of undoped TiO_2 is above the H^+/H_2 energy level. This situation is represented in Figs. 6 and 12.

Fig. 22 shows the dynamics of a TiO_2-based PEC with an applied chemical bias. The related electrochemical chain is shown in Fig. 23.

With a $\Delta pH = 14.6$, Eq. (20) yields an imposed voltage of 0.86 V during the first cycle of the experiment (1.56 –0.70 V). Consequently, the EMF data recorded for both PECs are relatively consistent.

8. Efficiency of photo-electrochemical cell

8.1. General issues

The efficiency of photo-electrochemical cells will be the main determining factor of hydrogen production costs using PEC technology. Consequently, the potential for commercialization of this technology will be likely to be determined largely by its costs compared to those of the conversion of methane according to the following reaction:

$$2H_2O + CH_4 \rightleftarrows 4H_2 + CO_2, \quad (25)$$

The cost of hydrogen generation using methane reforming technology is US$0.65/kg [1]. The cost of hydrogen generated using PEC technology is not available at present since this technology is not yet at the stage of commercial maturity. Intensive research activities aim at increasing the efficiency of this technology and, in particular, decreasing the energy losses when converting solar energy into chemical energy (viz., hydrogen) [125].

8.2. Energy losses

8.2.1. Major components

The energy losses associated with energy conversion using PECs include several components that are associated with the following effects:

- Photons with energies lower than E_g are not absorbed. Fig. 24 shows the fraction of the solar energy spectrum with photon energy $E_{ph} \geqslant E_g$ vs. E_g. This fraction is available for conversion.
- While photons with energy $\upsilon \geqslant E_g$ are absorbed, the energy in excess of E_g is dissipated as heat and, consequently, only a fraction of photon energy is efficiently used for conversion.

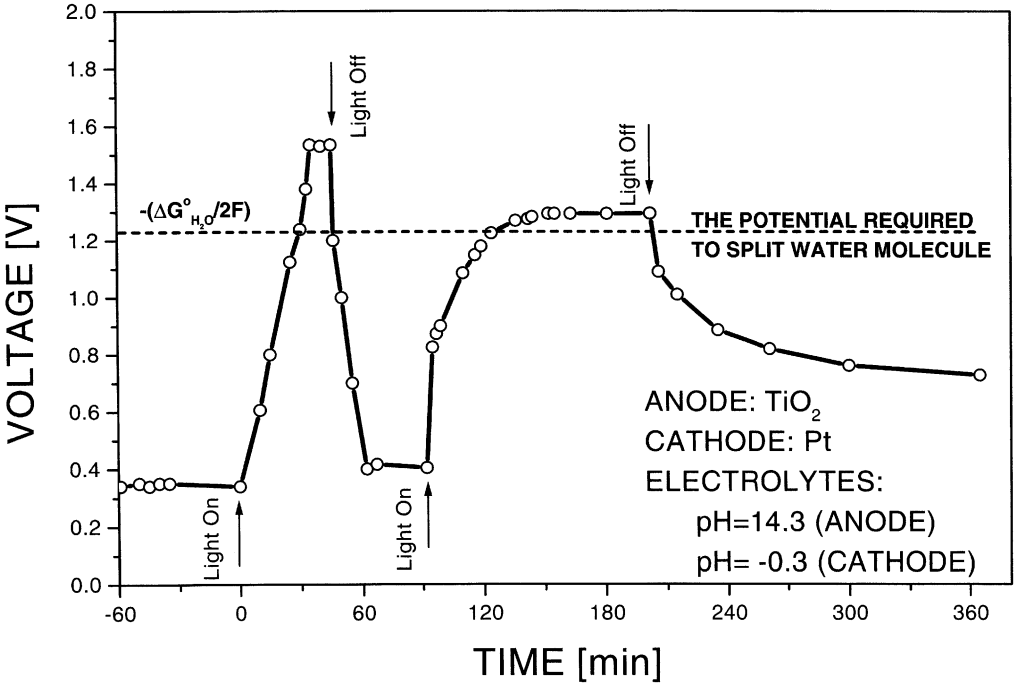

Fig. 22. Dynamics of PEC consisting of TiO_2 ceramic as photo-anode, Pt as cathode, aqueous solution of HCl as anodic electrolyte, and aqueous solution of KOH as cathodic electrolyte during light-on and light-off regimes [124].

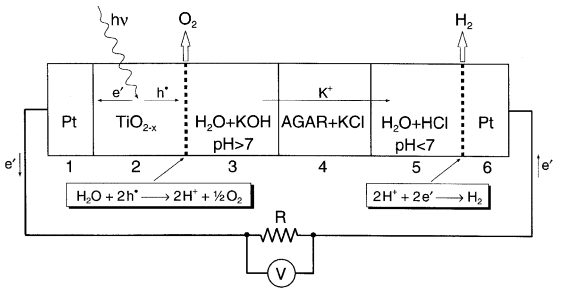

Fig. 23. Electrochemical chain of PEC used to generate data in Fig. 22.

- The energy of the excited state thermodynamically is internal energy rather than Gibbs free energy. Only 75% of the internal energy may be converted into chemical energy, while the remaining 25% constitute entropy-related losses [126].
- Fig. 25 shows that there are optical energy losses associated with different types of reflection and absorption.
- There are irreversible processes associated with (i) recombination of the electron–hole pairs, (ii) ohmic resistivity of the electrodes and electrical connections, and (iii) over-potentials at the electrode/electrolyte interface.

8.2.2. Definition of terms

The overall efficiency of a PEC unit, which is known as the *solar conversion efficiency* η_c, has been defined by Parkinson [127] according to the following expression:

$$\eta_c = \frac{\Delta G^0(H_2O)R(H_2) - V_{bias}I}{I_r A}, \tag{26}$$

where $\Delta G^0(H_2O)$ is the standard free enthalpy (Gibbs free energy of formation for 1 mol of liquid H_2O = 237.141 kJ/mol) [128], $R(H_2)$ the rate of hydrogen generation (mol/s), V_{bias} the bias voltage applied to the cell (V), I the current within the cell (A), I_r the incidence of solar irradiance, which depends on geographical location, time, and weather conditions (W/m^2), A the irradiated area (m^2).

With a known value for $\Delta G^0(H_2O)$ and the fact that $R(H_2) = I/F$, then Eq. (26) assumes the form:

$$\eta_c = \frac{I(1.23 - V_{bias})}{I_r A}. \tag{27}$$

All of the quantities in Eq. (27) may be determined experimentally, so it may be used for evaluation of the overall efficiency η_c.

The determination of the I_r requires knowledge of the air mass AM. It has been proposed to assume a value of $I_r = 970\ W/m^2$ as the standard level, corresponding to an AM of 1.5 [63].

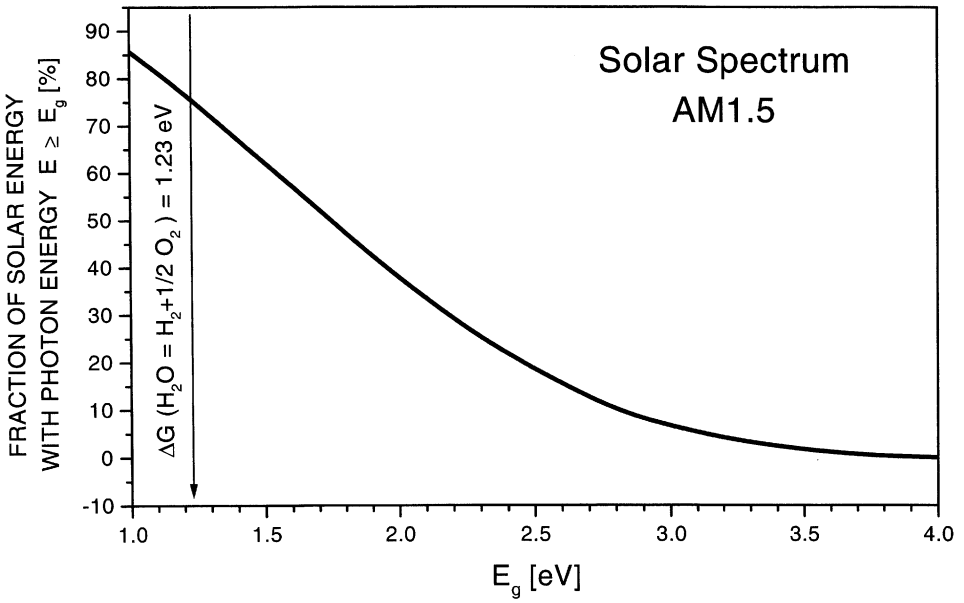

Fig. 24. Fraction of solar spectrum used efficiently for generation of electron–hole pairs vs. band gap.

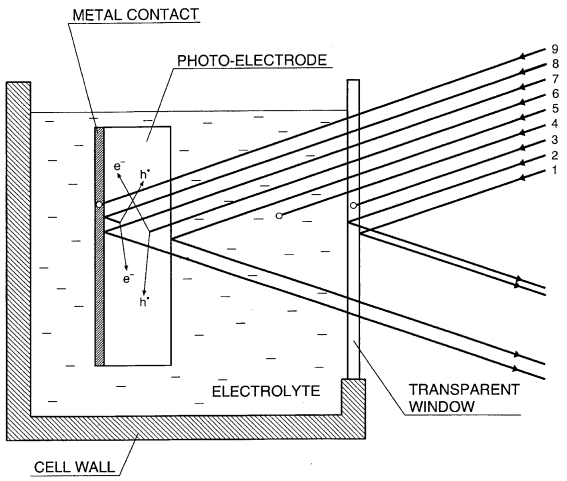

Fig. 25. Illustration of optical losses in PEC: (1) reflection from window external surface, (2) reflection from window internal surface, (3) absorption by window, (4) absorption by electrolyte, (5) reflection from surface of photo-anode, (6) photon absorbed by photo-anode and efficiently used for generation of electron–hole pair, (7) reflection from surface of metal contact, (8) reflection from surface of metal contact and efficiently used for generation of electron–hole pair, (9) absorption by metal contact.

Eqs. (26) and (27) are general expressions associated with the overall value of η_c; they cannot be related to specific aspects of the PEC, such as the properties of the electrodes and electrolyte, structure of the PEC, and the nature of the solar radiation. Therefore, the overall efficiency η_c cannot be used for guidance in the optimization of PEC performance unless the characteristics of the above-mentioned components of the PEC are well defined [129]:

$$\eta_c = \eta_g \eta_{ch} \eta_{QE}, \tag{28}$$

where η_g is the solar irradiance efficiency, η_{ch} the chemical efficiency, η_{QE} the quantum efficiency.

The η_g is defined as the fraction of the incident solar irradiance with photo-energy $\geqslant E_g$ and may be expressed as

$$\eta_g = \frac{J_g E_g}{E_S} = \frac{E_g \int_{E_g}^{\infty} N(E)\,dE}{\int_0^{\infty} EN(E)\,dE}, \tag{29}$$

where J_g is the flux density of absorbed photons.

The chemical efficiency is defined as the fraction of the excited state energy effectively converted to chemical energy and may be expressed as

$$\eta_{ch} = \frac{E_g - E_{loss}}{E_g}, \tag{30}$$

where E_{loss} is the energy loss per molecule in the overall conversion process.

For ideal systems, E_{loss} is defined as the difference between the internal energy and Gibbs free energy of the excited states. For real systems, E_{loss} assumes considerably larger values.

The quantum efficiency is defined as the ratio:

$$\eta_{QE} = \frac{N_{eff}}{N_{tot}}, \tag{31}$$

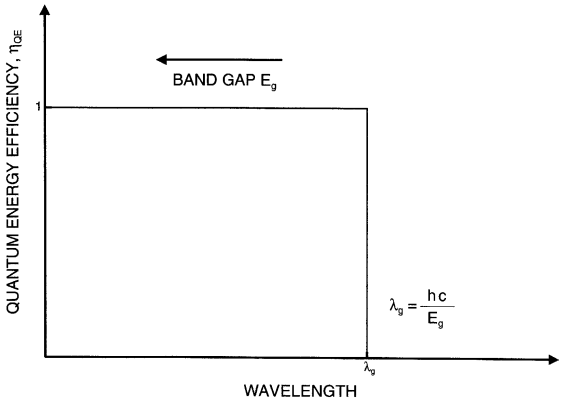

Fig. 26. Quantum energy conversion efficiency vs. wavelength for ideal case.

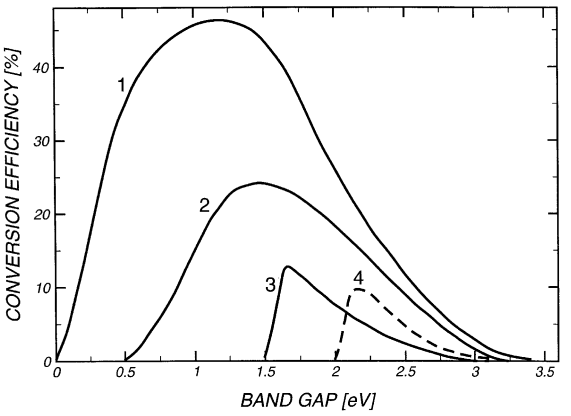

Fig. 27. Conversion efficiency of solar energy vs. band gap according to Gerischer [74]: (1) hypothetical efficiency without any losses, (2) efficiency including losses in semiconducting electrode, (3) efficiency of PEC with two photo-electrodes, (4) efficiency of PEC with one photo-electrode.

where N_{eff} is the number of effective incidents leading to the generation of photo-electron/photo-hole pairs, N_{tot} the total number of absorbed photons.

Fig. 26 illustrates the dependence of the quantum efficiency on the wavelength for the ideal case, where all photons of energies $\geqslant E_g$ are effective in ionization. As seen, the maximal quantum efficiency ($\eta_{QE} = 1$) is achieved for the wavelength (λ_g) with a photon energy equal to or larger than the band gap.

8.2.3. Effect of band gap on losses in energy conversion

Fig. 27 shows the conversion efficiency of solar energy at different levels of losses [74].

Curve 1 in Fig. 27 represents a hypothetical conversion efficiency η_g (solar irradiance efficiency for AM of 1.0) for the case of effective light absorption that ignores the losses due to charge transport within the semiconducting material and those resulting from over-potentials in the electrolyte (first two bulleted items in Section 8.2.1). As seen, the maximal value of solar irradiance efficiency η_g corresponds to semiconductors of $1.0 \leqslant E_g \leqslant 1.4$ eV.

Curve 2 in Fig. 27 represents the overall conversion efficiency η_c (solar conversion efficiency), in this case, including the losses due to charge transport in the solid state but still ignoring the losses in the electrolyte. This curve represents the case of energy conversion involving the following processes:

- Transport of electrons within solid (from the near-surface location of their generation inwards into the bulk) and, in particular, across the band bending (see Fig. 6), which is required for charge separation in order to prevent recombination. The estimated energy loss of these types of transport is ~ 0.2 eV.
- Transport of electrons from photo-anode to cathode. The related energy loss, which is equal to the difference between the E_c and E_F (see Fig. 6), is determined by the position of the donor level. The estimated loss of this type of transport is ~ 0.1 eV.
- Transport of electron holes from the position of their generation at the near-surface outwards to the photo-electrode/electrolyte interface (see Fig. 6). The estimated energy loss of this type of transport is ~ 0.2 eV.
- Charge transport within the electric circuit of the cell. The estimated loss of this type of transport is related to the Joule heating (I^2Rt, where t is the time).

As seen, the maximum in curve 2 corresponds to $1.4 \leqslant E_g \leqslant 1.6$ eV. This curve, which represents the ideal limits for photovoltaic energy conversion [63], is shifted toward higher E_g relative to curve 1. This illustrates the impact of band gap on energy losses.

Curves 3 and 4 in Fig. 27 represent the overall conversion efficiency η_c (solar conversion efficiency), taking into account all types of losses for PECs constructed using one photo-electrode or two photo-electrodes, respectively. In this case the energy losses take into account the evolution of gases at the electrodes and they are related to the cathodic and anodic over-voltages. The values of these losses are a complex function of the (i) mechanisms of the electrode reactions, (ii) current density, (iii) structures of the electrodes, (iv) surface properties of the electrodes, (v) temperature, (vi) composition of the electrolyte, and other relevant factors. The energy term (ΔG_{loss}), related to the energy losses due to these overvoltages, may be expressed by the following expression [74]:

$$|\Delta G_{\text{loss}}| \geqslant 0.5 + e(U_a + U_c + IR) \quad [eV], \tag{32}$$

where U_a is the over-potential at the anode, U_c the overpotential at the cathode.

The variables in Eq. (32) were determined experimentally by Gerischer [74], where curves 3 and 4 in Fig. 27 represent these data. As seen, the efficiency of the energy conversion of a cell involving only one photo-electrode (curve 4) is lower than that for a PEC with two electrodes (curve 3). Consequently, the implementation of a second photo-electrode should lead to an increase in efficiency from $\sim 9\%$ (curve 4) to $\sim 12\%$ (curve 3).

The efficiency of a PEC unit may also evaluated by so called incident photon-to-current conversion efficiency (IPCE) which is defined by the number of electrons generated by light in the external circuit divided by the number of incident photons [51,74]:

$$\mathrm{IPCC} = \frac{1250 \times \text{photocurrent density } [\mu\mathrm{A/cm^3}]}{\text{wavelength } [\mathrm{mm}] \times \text{photonflux } [\mathrm{W/m^2}]}, \qquad (33)$$

where the number 1250 is the unit conversion factor.

8.3. Progress in R&D

The intensity of research on materials for photo-assisted water decomposition, aiming at the development of PEC technology, is increasing rapidly. In order to achieve success, the focal points are likely to remain as materials selection, types of electrolytes, and the structure of the PEC units. The end-products must address the following requirements:

- the photo-electrodes must exhibit high energy conversion efficiencies;
- the PEC units must be durable and of low maintenance;
- the costs of manufacturing of the PEC units must be low.

The aim of the present section is to consider the reported data on energy conversion efficiencies. At present, there are insufficient data to allow a meaningful discussion on the durability of photo-electrodes and PEC units. Also, little is known of the costs of PEC units because their development has been limited to the laboratory scale.

Table 1 summarizes the current progress in the development of PECs in terms of selection of cell components and achieved efficiencies. These data have been selected because they report the impact of different PEC designs on the energy conversion efficiencies [7,9,12–14,16,18,25,26,75,76,95,123,130–137]. The energy efficiency is reported in terms of either total energy conversion efficiency (η_c) or quantum energy conversion efficiency (η_{QE}). By necessity, the latter assumes much higher values (see Eq. (28)).

Care must be taken when comparing the reported data owing to the use of different experimental conditions, including incident solar irradiance, light energy, light spectrum, photo-anode material, photo-anode processing conditions, cathode, and electrolyte. Further, many different light sources were used to produce radiation. There also are three reports of data using direct solar radiation [9,79,124].

In order to simplify such comparisons, the data in Table 1 are limited mainly to PECs with photo-anodes consisting of semiconducting materials and cathodes consisting of Pt (with one exception [131]). It can be seen that the energy conversion efficiency of direct solar energy (η_c) using a PEC equipped with an undoped TiO_2 photo-anode has been measured to be 0.4% [9,79]. Thus, this efficiency is comparable for both thin film [9] and single crystal [79] morphologies. Doping of TiO_2 with Cr or Al resulted in a slight increase in η_c (to 0.44 and 0.6%, respectively) [79]. Doping with other ions, such as Y, V, Cu, or Ta, did not lead to essential changes in the energy conversion efficiency [81].

Mavroides et al. [13] reported results for quantum energy conversion efficiencies for different TiO_2 specimens, including single crystals, polycrystals, thin films, and thin TiO_2 layers formed on metallic Ti through oxidation. These data indicated that the TiO_2 layers formed by oxidation on metallic Ti exhibited the best performance.

The application of an external bias (chemical or electrical) typically has resulted in a substantial increase in energy conversion efficiency. Akikusa and Khan [134], who studied TiO_2 single crystals, reported much larger values ($\eta_c = 1.6\%$), which were achieved through the application of a chemical bias ($\Delta pH = 15.5$, which is equivalent to 0.91 V). Even more impressively, the total energy conversion efficiency reported by Nozik [14], also for TiO_2 single crystals, was 10%, again with the application of chemical and electrical biases as well as UV light.

Studies on the performance of $SrTiO_3$ single crystals have revealed that the total energy conversion is very high—up to 20 [16] or 25% [25] without the application of a bias [16]. However, these data were obtained using high-energy lights of specific wavelengths. At present, only PECs based on $SrTiO_3$ as the photo-anode have been shown to exhibit EMF values that are sufficient for water decomposition without a bias. Very high total energy conversion efficiencies (in the range 12–18%) have been reported for photo-electrodes made of non-oxide materials, including GaAs and Al-doped GaAs [52,53]. However, these reports provided no information about the stability of the photo-cell performance or the effect of corrosion on the EMF of the photo-electrodes. While photosensitizers of organic compounds gave energy conversion efficiences up to 4.46%, they exhibit little stability in aqueous environments [121,122]. Therefore, there is a need to develop the sensitizers which not only display increased energy conversion but also exhibit a stable performance in aqueous solutions.

Unfortunately, the energy conversion data given in other reports are limited to quantum efficiencies (η_{QE}). The absence of the data necessary to calculate η_c using the other factors in Eq. (28) (η_g and η_{ch}) preclude the possibility of the calculation of the energy conversion efficiency.

The aim of a PEC is to harvest the solar energy. Therefore, data obtained using the solar energy spectrum are the most appropriate for comparison in terms of practical

Table 1
Experimental data on efficiencies of photo-electrochemical cells of different structures

Authors	Cell structure	Efficiency	Light source
Fujishima and Honda [7]	a: TiO_2 (SC) c: Pt-black e: Fe^{+3} ions	$\eta_{QE} = 10\%$	500 W Xe lamp Several mA/cm^2
Fujishima et al. [9]	a: TiO_2 (OX) c: Pt-black + H_2 (NHE) e: 1 M NaOH (a)/0.5 M H_2SO_4 (c)	$\eta_c = 0.4\%$	Sunlight
Ohnishi et al. [12]	a: TiO_2 (SC) c: Pt c: 0.5 M K_2SO_4 + 0.05 M CH_3COOH + 0.05 M CH_3COONa	$\eta_c = 0.27\%$ $\eta_{QE} = 6.1 \times 10^{-1}\%$ (0.105 mW) $\eta_c = 0.029\%$ $\eta_{QE} = 6.7 \times 10^{-2}\%$ (1.040 mW) $\eta_c = 0.014\%$ $\eta_{QE} = 3.2 \times 10^{-2}\%$ (3.200 mW)	500 W Hg lamp $\lambda = 365$ nm
Mavroides et al. [13]	(1) a : TiO_2 (SC) c:Pt e : pH = 8 (2) a: TiO_2 (PC) c:Pt e : pH = 8 (3) a: TiO_2 (TF) c:Pt e : pH = 8 (4) a: TiO_2 (OX) c:Pt e : pH = 13	λ (nm) / η_{QE} (%): SC (1) / PC (2) / TF (3) / OX (4) 350: 30 / 25 / 80 / 42 310: 81 / 60 / 70 / 80 275: 65 / 38 / 35 / 72 250: 22 / 17 / 08 / 57	1000 W Xe Lamp
Nozik [14]	a : TiO_2(SC) c: Pt e: (1) 1 M Phosphate buffer (pH = 6.5) (2) 0.1 M KOH (3) 0.1 M H_2SO_2 (4) 0.1 M KOH (a)/0.2 M H_2SO_4 (c)	Bias (V) / η_c (%): (1): 0.8 / 2.4 (1): 0.5 / 1.0 (2): 1.0 / 3.4 (2): 0.6 / 3.2 (3): 0.8 / 4.1 (3): 0.6 / 2.4 (4): 0.0 / 9.5 (4): 0.4 / 10.1	UV light (300–400 nm) 26 mW/cm^2
Wrighton et al. [16]	a : $SrTiO_3$ (SC) c: Pt e : 9.5 M NaOH	λ (nm) / Intensity (Ein/min) / η_{EQ} (): 351: 8.2×10^{-7} / 11 313: 1.4×10^{-7} / 100 254: 1.1×10^{-7} / 96 $\eta_c = 20\%$ ($\lambda = 330$ nm)	(1) Ar ion laser (2) 200 W Hg arc lamp
Morisaki et al. [17]	a: Hybrid TiO_2–Si solar cell c: Pt e : 0.1 M NaOH	$\eta_c = 0.1\%$	500 W Xe lamp

Table 1. (*Continued*)

Authors	Cell structure	Efficiency			Light source
Watanabe et al. [18]	a : $SrTiO_3$ (SC) c: Pt e : 1 M NaOH (a)/0.5 M H_2SO_4 (c)	$\eta_{QE} = 20\%$ ($\lambda = 350$ nm) $\eta_{QE} = 0.4\%$ ($\lambda = 380$ nm)			500 W Xe lamp
Okuda et al. [131]	a: (1) $BaTiO_3$ (PC) (2) $SrTiO_3$(PC) c: Pt e: 1 M KOH	$\eta_c = 0.0068\%$ $\eta_c = 0.043\%$			500 W Xe lamp
Laser and Bard [132]	a : TiO_2 (TF) c: Teflon $+O_2$ e: 5 M NaOH or 5 M $HClO_4$	$\eta_{QE} = 26\%, \eta_c = 1$–$2\%$ ($\lambda = 365$ nm)			450 W Xe lamp
Mavroides et al. [25]	a : $SrTiO_3$ (SC) c: Pt e : 10 M NaOH	Bias V 0 0.3 0.9	η_{EQ} 10 20 80	η_c ($\lambda = 325$ nm) 5% 20% 25%	Photon 3.8 eV
Fleischauer and Allen [26]	a : TiO_2 (TF–250 nm) c: Pt e: Electrolyte of pH = 4 (a)/1 M H_2SO_4 (c)	Visible light: $\eta_c = 0.2\%$ UV: $\eta_c = 2\%$			Visible and UV (1) 150 W Xe arc lamp (2) 5*O*0 W Xe arc lamp
Giordano et al. [95]	a : TiO_2 (OX—1 mm); c: Pt e: Aqueous solutions of mixtures of $TiCl_3$, $MgCl_2$, $Mg(NO_3)_2$, HCl, and H_2PtCl_6 (bias = 0.5 V)	$\eta_c = 0.13$–2%			4*O*0 W Hg lamp
Guruswamy et al. [132]	a: (1) La_2O_3–Cr_2O_3 (TF) deposited on Ti (2) La_2O_3–RuO_2 (TF) deposited on Ti c: Pt e : 0.5 M H_2SO_4	V_{bias} (V) 0.5 1.0 1.25	(1) η_c (%) 0.1 0.6 1.2	(2) η_c (%) 0.08 4.0 4.6	Xe arc lamp 0.22 W/cm^2
Yoon and Kim [133]	a : $SrTiO_3$ (PC–0.2 mm) c: Pt e : 1 M NaOH	$\eta_{QE} = 3.5\%$			150 W halogen lamp (340 nm)

Ghosh and Maruska [79]	a: (1) Undoped TiO_2 (SC), (2) Al-doped TiO_2 (SC–0.05 wt) (3) Cr-doped TiO_2 (SC–0.004 wt) c: Pt e : 5 M KOH	(1) $\eta_c = 0.4\%$ (2) $\eta_c = 0.6\%$ (2) $\eta_c = 0.44\%$	Sunlight 105 mW/cm^2
Houlihan et al. [81]	a: (1) Undoped TiO_2 (TF—2–3 μm) (2) Y-doped TiO_2 (TF—2–3 μm/100 ppm) (3) V-doped Y-doped TiO_2 (TF—2–3 μm/100 ppm) (4) Cu-doped TiO_2 (TF—2–3 μm/100 ppm) (5) Al-doped TiO_2 (TF—2–3 μm/100 ppm) (6) Ta-doped TiO_2 (TF—2–3 μm/100 ppm) c: Pt e : 1 M NaOH (a)/0.5 MH_2SO_4 (c)	$\eta_c(Y) > \eta_c(V) > \eta_c(Cu) > \eta_c(A1) > \eta_c(Ta) > \eta_c$(undoped) $\eta_c(Y) = 0.4\%$ η_c(undoped) = 0.56%	1000 W Xe lamp
Prasad et al. [100]	a : TiO_2–In_2O_3 (SC) c: Pt e : 1 M NaOH	$\eta_{QE} = 100\%$	1000 W Xe–Hg lamp
Bak et al. [124]	a : TiO_2(OX) c: Pt e: (1) 0.5 M Na_2SO_4 (2) 4 M KOH (a)/4 M HCl (c)	$\eta_c = 0.4\%$ (estimate) (attained 20–25 min after initial light exposure)	Sunlight
Akikusa and Khan [134]	a : TiO_2 (SC) c: Pt e : 5 M KOH (a)/3 M H_2SO_4 (c); $\Delta pH = 15.5$	$\eta_c = 1.6\%$	150 W Xe arc lamp
Khaselev et al. [52]	a:p-GaAs/n-GaAs/p-$Ga_{0.52}In_{0.48}P$ (TF–500 nm) c: Pt e : 3 M H_2SO_4 + 0.01 M t-octylphenoxypolyethoxyethanol	$\eta_c = 12.4\%$	150 W tungsten–halogen lamp (1.19 W/cm^2)
Licht et al. [53]	a : AlGaAs/$SiRuO_2$ (TF) c: Pt-black e : 1 M $HClO_4$	$\eta_c = 18.3\%$	50 W tungsten–halogen lamp 0.135 W/cm^2
El Zayat et al. [123]	a: Zr-doped $SrTiO_3$ (SC) c: Pt e : 5 M NaOH + 15 μM dye Dyes: (1) safranin ($C_{20}H_{19}N_4Cl$) (2) fluorescin ($C_{20}H_{12}O_5$) (3) eriochrome black T ($_{20}H_{12}N_3NaO_{75}$)	Without dyes: $\eta_c = 1.4\%$ With dyes (1) $\eta_c = 4.46\%$ (1) $\eta_c = 3.87\%$ (1) $\eta_c = 3.9\%$	Halogen lamp : 1000 W 23 mW/cm^2

a = anode; c = cathode; e = electrolyte; SC = single crystal; PC = polycrystalline ceramic; TF = thin film; OX = TiO_2 oxidation layer on Ti.

applications. It is clear that the energy conversion efficiencies obtained using specific energy sources, where the energy spectrum differs from that of solar energy, may be substantially larger than that from solar energy when applied light sources of higher energies are used. Accordingly, the use of ultraviolet (UV) light results in a substantial increase on the energy conversion efficiency [26].

It appears that the only study to report the dynamics of PEC performance, irrespective of the light source, is that of Bak et al. [124]. These data showed that the photo-electric effect is characterized by an inertial effect, which was shown by a time lag of 20–25 min between exposure to sunlight and appearance of the maximal EMF value.

Very little is known of the durability of PEC units, which is an issue that must be addressed before evaluation of commercial potential can be made. With the present state of knowledge of oxide materials, it appears that PECs equipped with photo-anodes based on TiO_2 and its solid solutions can be expected to exhibit the best durability. Therefore, these materials may be the optimal candidates for photo-anodes, assuming that the energy conversion efficiencies can be increased sufficiently.

9. Impact of hydrogen technology on environment

In principle, the use of hydrogen as a fuel for vehicular power, electricity generation, and heating results in near-zero emissions of greenhouse gases. The prognoses for the impact of hydrogen technology on the emission of greenhouse gases are available mainly for vehicles, which are expected to be the primary mass-market products.

Fig. 1 shows relative emissions of greenhouse gases (expressed in the amount of carbon emitted per km) for today's gasoline-powered internal combustion engine vehicles (ICEV) in comparison to vehicles powered by fuel cells using hydrogen and other fuels [138]. It is clear that fuel cell technology offers very substantial improvements in emission levels of greenhouse gases, although emissions from the combustion of conventional fuels (gasoline, methanol, natural gas) still are substantial. In contrast, the combustion of hydrogen in a fuel cell—when the hydrogen is obtained from renewable sources (solar, wind, tidal, hydroelectric, hydrothermal)—is the optimal technology from the environmental point of view. Consequently, it may be expected that hydrogen-powered vehicles using fuel cells will overtake the market in the near-future.

An alternative not covered in Fig. 1 is the addition of hydrogen to natural gas [138]. The addition of only 5 vol% hydrogen to natural gas results in a substantial reduction of NO_x emissions. However, CO_2 still is produced during combustion.

At present, there is a paradox between the efforts of vehicle manufacturers, who argue that hydrogen-fuelled cars must be produced in order to reduce greenhouse gas emissions, and the state of the technology necessary to produce, transport, and store environmentally friendly hydrogen. While research and development in automobile engines and fuel cells proceed rapidly, the technology to produce hydrogen using renewable sources of energy still is only at the preliminary experimental stage; the technologies for hydrogen storage and transportation are more advanced but not adequate for the expected range of applications. The inevitable result of the failure of these four technologies to be developed synchronously will result in the proliferation of hydrogen-fuelled vehicles in demand of large-scale hydrogen sources. This vacuum almost certainly will be filled by the hydrogen produced from techniques that can provide large amounts of hydrogen but at the cost of the emission of greenhouse gases during production. The two most likely methods to become entrenched are:

- steam reforming of methane, which results in CO_2 emissions;
- water electrolysis using electricity generated from fossil fuels, which also produces CO_2.

10. Hydrogen economy

At present, the market cost of hydrogen obtained from steam reforming of methane is 65 US cents per kg [1]. This technology results in greater emissions of CO_2 than the direct combustion of methane [5]. Approximately 95% of the total hydrogen production in the US is based on steam reforming technology [1]. Therefore, steam reforming can be viewed as a technology that already is entrenched.

It is not possible to predict the price of hydrogen produced from water using solar energy. The recent report of Morgan and Sissine [1] indicates that efficiencies in the range 10–15% may be economical. The critical issue in the development of PECs of such efficiencies is the processing of the photo-electrode. If inexpensive, effective, and corrosion-resistant photo-electrodes become available, then commercially viable PECs can be produced since the ancillary components can be engineered with existing technologies.

Thomas et al. [138] have predicted that the price of cars powered by hydrogen fuel cells will be higher by only US$1100 compared to today's ICEV and less expensive than other fuel cell vehicles (FCV) using methanol or gasoline, as shown in Fig. 28. According to these estimates, the production of hydrogen FCV will result in higher internal return on investment than that of cars powered by gasoline fuel cells. The estimates also indicate that hydrogen FCV will have substantially better fuel economies as well.

Fig. 29 shows predictions for the scale of hydrogen production, where there is anticipated to be a substantial increase in hydrogen production beginning in 2010 [138], presumably driven by the relative costs of hydrogen and gasoline. One should expect that this will lead to a drastical

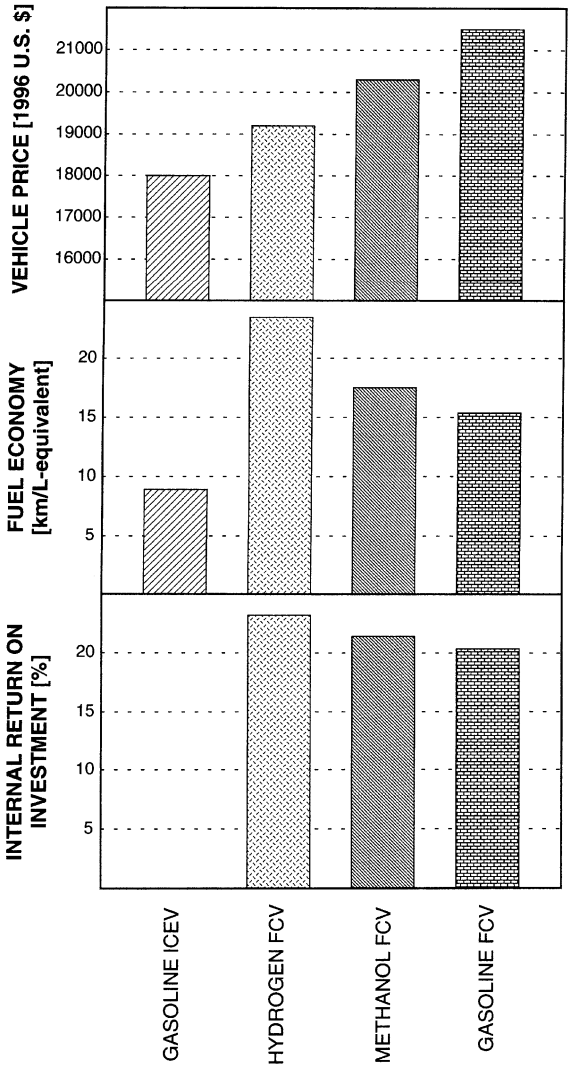

Fig. 28. Prediction of vehicle price, fuel economy, and return on investment [138].

increase in carbondioxide emission (curve 1 in Fig. 30). Although this estimate does not indicate the proportion of hydrogen produced from renewable sources, it can be expected that this level of demand will fuel research and development into alternative methods of hydrogen production.

Likewise, increasing recognition of the environmental consequences of greenhouse gas emissions can be expected to drive the development of the production of hydrogen from water using solar and other renewable energy sources.

In a recent development, the race to development hydrogen technology has expanded beyond the global realm. A substantial research project recently has been initiated by the National Space Development Agency (NASDA) of Japan

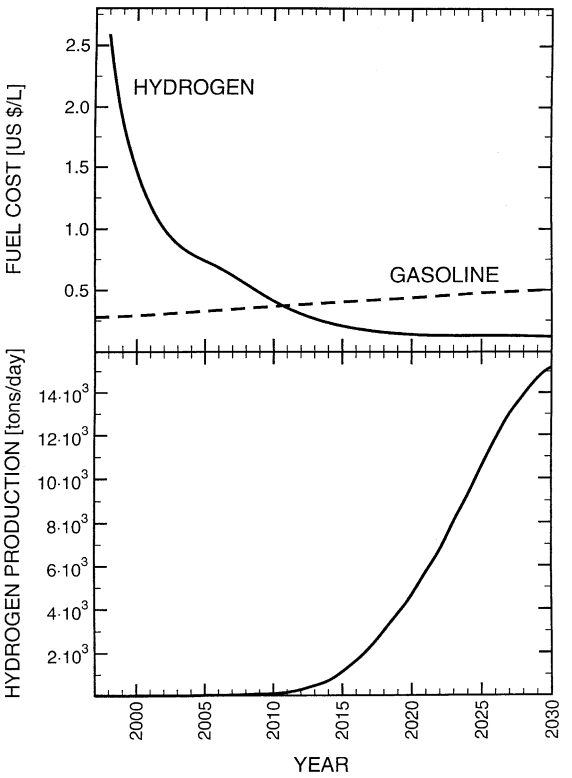

Fig. 29. Fuel cost (gasoline and hydrogen) and hydrogen production in period 2000–2030 [138].

and the Institute for Laser Technology (ILT). Its aim is the development of hydrogen generation technology using a space-based solar unit that will harvest solar energy [139]. This technology will involve the following three devices:

- space-based solar condenser collecting solar energy;
- laser generator transforming the solar beam into a laser beam and sending it to a groundbased photo-catalytic device;
- ground-based photo-catalytic device consisting of a TiO_2 powder suspended in water to produce oxygen and hydrogen.

This proposed technology has the following advantages over existing technologies based on solar energy collected on the Earth's surface:

- solar irradiance in space is free of energy losses due to energy absorption by the atmosphere and so is substantially larger than that on the earth surface;
- solar energy in space is available continuously and independently of the diurnal cycle;
- solar energy in space is available independently of weather conditions, although the laser beam would be affected somewhat.

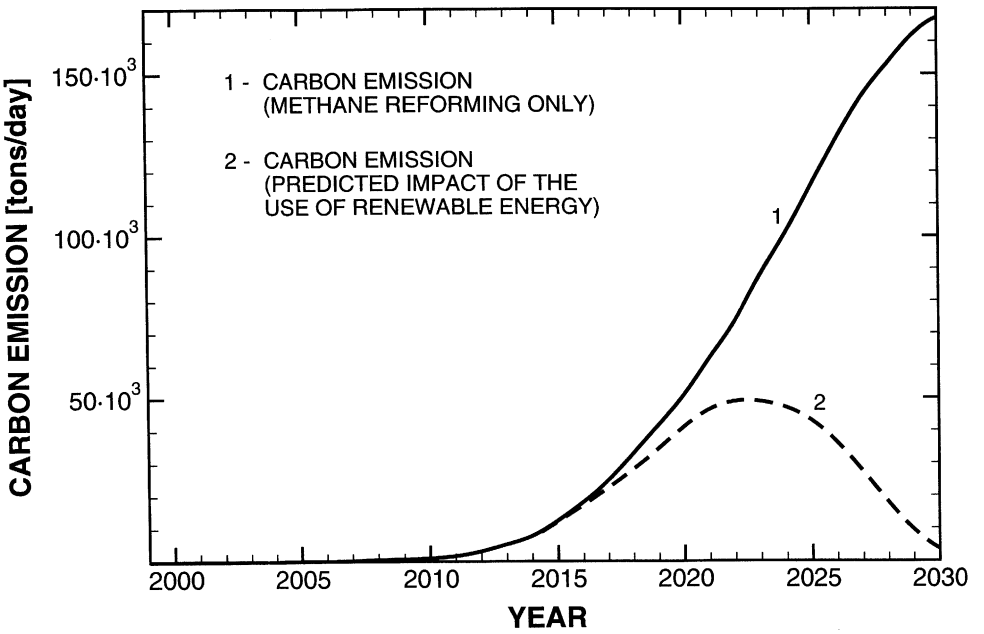

Fig. 30. Predicted increase of carbon emission (based on data of Thomas et al. [138]); (1) assuming methane reforming, (2) predicted impact of the use of renewable energy.

A disadvantage of this technology is that a photo-catalytic device produces a mixture of hydrogen and oxygen, which must be separated by an electrochemical device (Section 2.3).

It has been claimed, based on preliminary estimates, that the cost of hydrogen manufactured using this technology will be a modest $\sim$ 20 Japanese yen for an amount of hydrogen equivalent to 1 l of gasoline. It is expected that the first experimental satellite will be launched by 2010 and the entire system will be completed by 2020.

11. Conclusions

In light of the preceding overview, the state of development of PECs may be summarized as follows:

- Oxide materials are the most promising photo-electrodes. Despite the relatively low efficiencies of energy conversion, these inexpensive materials exhibit good corrosion-resistance and, consequently, are expected to exhibit stable performance over extended periods of time.
- Although PECs based on TiO_2 and its solid solutions exhibit EMF values that are lower than that required for water decomposition (0.7–0.9 V) [124], the majority of reports concern the materials-based on TiO_2. This interest is a product of the fact that TiO_2 has the best corrosion-resistance of oxide materials, despite the requirement of the imposition of a bias voltage.
- PECs based on $SrTiO_3$ are the only cells that do not require any bias because its EMF is above that required for water decomposition. Unfortunately, its energy conversion efficiency is very low ($< 0.1\%$) due to its relatively large band gap (3.4 eV) [73].

These photo-electrodes fall into two groups of materials. The first group includes ionic compounds, such as oxide materials. Although, at present, these exhibit low energy conversions ($\leqslant 0.6\%$), their corrosion-resistance is high. The second group includes valence semiconductors, such as GaAs. Although these exhibit high energy conversions ($\leqslant 18\%$), they are readily subject to corrosion in aqueous environments. It is likely that photo-electrodes that are less efficient but long lasting will prove to be the successful commercial alternative.

It has been shown that the development of PEC technology will be determined by the development of processing technology for photo-electrodes that must satisfy several materials requirements. Such photo-electrodes must exhibit very specific semiconducting and electrochemical properties. Although the most important properties have been identified, it is difficult to obtain materials that meet all of the requisite materials properties that will achieve photo-electrodes of maximal performance. Thus, a sophisticated material such as a photo-electrode will require an equally sophisticated understanding of its processing, properties, and performance. The successful development of this technology will require the accumulation of a large body of empirical data needed for the

optimization of processing photo-electrodes of desired properties.

The framework by which such an understanding will be gained will be based upon the novel semiconducting properties of photo-electrodes. Specifically, suitable performance characteristics will result from the appropriate processing, which will involve the imposition of specific defect chemistry [140]. A promising issue in the development of photo-electrodes is the application of low-dimensional interface structures that exhibit outstanding properties not displayed by the bulk phase [56,57]. Specifically, there is a need to understand the local properties of interface, such as grain boundaries, on performance of photo-electrodes. It has been shown that the charge transport within the interface layer of TiO_2 is entirely different from that of the bulk phase [141].

Dye sensitization is very promising in processing photo-electrodes that exhibit an increased energy conversion [142], however, there is a need to develop sensitizers that exhibit a stable performance in aqueous solutions.

The development of the technology of hydrogen generation from water using solar energy offers three important advantages in comparison to other similar technologies:

- this technology offers a fuel that is totally clean, both during its production and its combustion, which is not the case with gasoline, methanol, or natural gas;
- solar power is universally available, while equally attractive alternatives (wind, tidal, hydroelectric, and hydrothermal power) are more regionally based;
- it is likely that this technology will be developed on a compact scale, where domestic versions of hydrogen generators will provide electricity, heating, and vehicular fuel on site.

In conclusion, this technology offers the opportunity to address the two global problems of (1) the increasing need to reduce emissions of greenhouse gases and (2) the requirement to develop alternative and renewable sources of energy.

12. Historical outline

1839: The Becquerel effect

The discovery of the photo-electrochemical effect was made by Becquerel in 1839 [143]. Studying the AgCl/electrolyte/metal system, he observed that a current flowed between the AgCl and the metal electrodes when AgCl was exposed to light. Since then, this effect has been termed the *Becquerel effect*. Discovery of this effect paved the way for PEC technology.

1954: Theory of photo-electrochemistry

The derivation of the theory of semiconductors, made by Brattain and Garret [144,145], has led to the theoretical explanation of the Becquerel effect. Brattain and Garret [144,145] explained the charge transport during the photo-electrochemical effect in terms of the band model of the electrodes.

The theory proposed by Brattain and Garret [144,145] subsequently was developed by Gerischer [146], Memming [147], and Morrison [58]. Their studies have led to a better understanding of the impact of the semiconducting properties of photo-electrodes on the photo-electrochemical effect.

1972: Hydrogen generation using PEC

Fujishima and Honda [7] first showed that a PEC may be used for hydrogen generation through the decomposition of water using a photo-anode of TiO_2. Although subsequent work showed that the use of TiO_2 requires the application of an external bias voltage [22,51,58], the work of Fujishima and Honda [7] indicated that the PEC method may be used to generate hydrogen using solar energy. They also showed that oxide materials, which are highly corrosion-resistant, may be used as the photo-electrodes.

1975: Oxide materials as photo-electrodes

The work of Fujishima and Honda [7] resulted in the search for other oxide materials as candidates for photo-electrodes that do not require an external bias for water decomposition [14,21,51,73]. These studies have shown that several oxide materials, including $KTiO_3$ and $SrTiO_3$, do not require an external bias, they exhibit light energy conversions that are substantially lower than that of TiO_2 [51].

1976: Complex electrode structures

Morisaki et al. [17] constructed a hybrid electrode consisting of a stack of a Si-based photo-voltaic unit plus a photo-anode made of TiO_2. Although Morisaki et al. [17] did not obtain an outstanding conversion efficiency, this concept represents an important development in PEC technology owing to the possibility of the application of an internal bias voltage generated at the underlayer Si cell. Similar cell structures based on this idea were patented subsequently in the USA [148,149].

Miller and Rocheleau [150] also reported the fabrication of a hybrid electrode involving an In–Sn oxide film as the contact between a photoactive semiconductor (TiO_2 or WO_3) and a Si solar cell, which resulted in an increase in energy conversion efficiency to $> 1\%$.

Further progress in the development of the light conversion efficiencies of PECs has been made with the use of two photo-electrodes, consisting of a photo-anode of an n-type

semiconductor and a photo-cathode of a p-type semiconductor [11,23].

1977-2001: Modification of TiO_2

After TiO_2 was identified as the best candidate for the photo-anode, it was shown that its light absorption may be increased substantially by modification of its semiconducting and electrochemical properties through doping with aliovalent ions and producing solid-solutions with other oxides [30,47,59,79–94,70,95–111].

Heterogeneous doping with nanoparticles of noble metals also has a beneficial effect on the performance of PECs [39,95,112–116].

Recent studies have shown that application of dyes leads to a substantial increase in light absorption and, consequently, to the conversion efficiency of the solar energy [117–123].

References

[1] Morgan D, Sissine F. Congressional Research Service, Report for Congress, The Committee for the National Institute for the Environment, Washington, DC 20006-1401, 28 April 1995.
[2] Nejat Veziroglu T. Int J Hydrogen Energy 1998;23:1077.
[3] Szyszka A. Int J Hydrogen Energy 1998;23:949.
[4] Mitsugi C, Harumi A, Kenzo F. Int J Hydrogen Energy 1998;23:159.
[5] The Economist Technology, Quarterly, March 25, 2001. p. 29.
[6] US Department of Energy, National Renewable Energy Laboratory. Hydrogen the fuel for the future, DOE/GO-1-95-099 DE95004024, March 1995.
[7] Fujishima A, Honda K. Nature 1972;238:37.
[8] Watanabe T, Fujishima A, Honda K. Chem Lett 1974;897.
[9] Fujishima A, Kohayakawa K, Honda K. J Electrochem Soc 1975;12:1487.
[10] Honda K. In: Ohta T, editor. Solar-Hydrogen Energy Systems. Oxford: Pergamon Press, 1979. p. 137–69.
[11] Yoneyama H, Sakamoto H, Tamura H. Electrochim Acta 1975;20:341.
[12] Ohnishi T, Nakato Y, Tsubomura H. Ber Bunsen Ges 1975; 79:523.
[13] Mavroides JG, Tchernev DI, Kafalas JA, Kolesar DF. Mater Res Bull 1975;10:1023.
[14] Nozik AJ. Nature 1975;257:383.
[15] Hodes G, Cahen D, Manessen J. Nature 1976;260:312.
[16] Wrighton MS, Ellis AB, Wolczanski PT, Morse DL, Abrahamson HB, Ginley DS. J Am Chem Soc 1976;98:2774.
[17] Morisaki H, Watanabe T, Iwase M, Yazawa K. Appl Phys Lett 1976;29:338.
[18] Watanabe T, Fujishima A, Honda K. Bull Chem Soc Jpn 1976;49:355.
[19] Butler MA, Nasby RD, Quinn RK. Solid State Commun 1976;19:1011.
[20] Bolts JM, Wrighton MS. J Phys Chem 1976;80:2641.
[21] Carey JH, Oliver BG. Nature 1976;259:554.
[22] Seraphin BO. In: Seraphin BO, editor. Solar energy conversion. Berlin: Springer, 1979. p. 5–56.
[23] Nozik AJ. Appl Phys Lett 1976;29:150.
[24] Dutoit EC, Cardon F, Gomes WP. Ber Bunsenges Ges 1976;80:475.
[25] Mavroides JG, Kafalas JA, Kolesar DF. Appl Phys Lett 1976;28:241.
[26] Fleischauer PD, Allen JK. J Phys Chem 1978;82:432.
[27] Memming R. Electrochim Acta 1980;25:77.
[28] Butler MA, Abramovich M, Decker F, Juliao JF. J Electrochem Soc 1981;128:200.
[29] Soliman AA, Seguin HJJ. Sol Energy Mater 1981;5:95.
[30] Kiwi J, Grätzel K. J Phys Chem 1986;90:637.
[31] Prasad G, Rao NN, Srivastava ON. Int J Hydrogen Energy 1988;13:399.
[32] Regan BO, Grätzel O. Nature 1991;353:737.
[33] Pandey RN, Babu KS, Singh D, Srivastava ON. Bull Chem Soc Jpn 1992;65:1072.
[34] Augustynski J. Electrochim Acta 1993;38:43.
[35] Sukampto JPH, McMillan CS, Smyrl W. Electrochim Acta 1993;38:15.
[36] Danny Harvey LD. Int J Hydrogen Energy 1996;21:583.
[37] Bolton JR. Sol Energy 1996;57:37.
[38] Pandey RN, Chandra-Babu KS, Srivastava ON. Prog Surf Sci 1996;52:125.
[39] Zhao G, Kozuka H, Yoko T. Sol Energy Sol Cells 1997;46:219.
[40] Zhao G, Utsumi S, Kozuka H, Yoko T. J Mater Sci 1998;33:3655.
[41] Hao Y, Yang M, Hu C, Cai S, Liu M, Fan L, Li Y. Sol Energy Mater Sol Cells 1998;56:75.
[42] El Zayat MY, Saed AO, El-Dessouki MS. Int J Hydrogen Energy 1998;23:259.
[43] Liu Y, Hagfeldt A, Xiao XR, Lindquist SE. Sol Energy Mater Sol Cells 1998;55:267.
[44] Stanley A, Verity B, Matthews D. Sol Energy Mater Sol Cells 1998;52:141.
[45] Pandey RN, Misra M, Srivastava ON. Int J Hydrogen Energy 1998;23:861.
[46] Gomez M, Rodriguez J, Tingary S, Hagfeldt A, Lindquist SE, Granquist CG. Sol Energy Mater Sol Cells 1999;59:277.
[47] Zhao G, Kozuka H, Lin H, Yoko T. Thin Solid Films 1999;339:123.
[48] Zhao G, Kozuka H, Lin H, Takahashi M, Yoko T. Thin Solid Films 1999;340:125.
[49] Kozuka H, Takahashi Y, Zhao G, Yoko T. Thin Solid Films 2000;358:172.
[50] Aranyos V, Grennberg H, Tingry S, Lindquist SE, Hagfeldt A. Sol Energy Mater Sol Cells 2000;64:97.
[51] Chandra S. Photoelectrochemical solar cells. NewYork: Gordon and Breach, 1985.
[52] Khaselev O, Turner JA. Science 1998;280:425.
[53] Licht S, Wang B, Mukerji S, Soga T, Umeno M, Tributsch H. J Phys Chem B 2000;104:8920.
[54] Hirschwald W. In: Nowotny J, Dufour L-C, editors. Surface and near-surface chemistry of metal oxides. Amsterdam: Elsevier, 1988. p. 61.
[55] Nowotny J. In: Nowotny J, Dufour L-C, editors. Surface and near-surface chemistry of metal oxides. Amsterdam: Elsevier, 1988. p. 281.
[56] Nowotny J. In: Nowotny J, editor. Science of ceramic interfaces. Amsterdam: Elsevier, 1991. p. 79.

[57] Nowotny J. In: Nowotny J, editor. Science of ceramic interfaces II. Amsterdam: Elsevier, 1994. p. 1.
[58] Morrison SR. Electrochemistry at semiconductor and oxidized metal electrodes. New York: Plenum Press, 1980. pp. 1–401.
[59] Nozik AJ. In: Heller A, editor. Semiconductor liquid-junction solar cells. Proceedings of the Conference on the Electrochemistry and Physics of Semiconductor Liquid Interfaces under Illumination. Virginia: Airlie, 1977. p. 272–92.
[60] Hoffmann MR, Martin ST, Choi W, Bahnemann DW. Chem Rev 1995;95:69.
[61] Hagfeldt A, Grätzel M. Chem Rev 1995;95:49.
[62] Oriel-Instruments. Book of Photon Tools, 1999. p. 1–3.
[63] Wenham SR, Green MA, Watt ME. Applied photovoltaics, Centre for Photovoltaic Devices and Systems, Sydney, 1994. p. 239–46.
[64] Chandra S. Photoelectrochemical solar cells. New York: Gordon and Breach, 1985. p. 98.
[65] Anderman M, Kennedy JH. In: Finklea HO, editor. Semiconductor electrodes. Amsterdam: Elsevier, 1988. p. 147–202.
[66] Chandra S. Photoelectrochemical solar cells. New York: Gordon and Breach, 1985. p. 163–9.
[67] Nanthakumar A, Amstrong NR. In: Finklea HO, editor. Semiconductor electrodes. Amsterdam: Elsevier, 1988. p. 203–40.
[68] Mizushima K, Tanaka M, Iida S. J Phys Soc Jpn 1972;32:1519.
[69] Mizushima K, Tanaka M, Asai A, Iida S, Goodenough JB. J Phys Chem Solids 1979;40:1129.
[70] Philips TE, Moorijani K, Murphy JC, Poehler TO. J Electrochem Soc 1982;129:1210.
[71] Nowotny J, Radecka M, Rekas M. J Phys Chem Solids 1997;58:927.
[72] Bak T, Nowotny J, Sorrell CC. In: Nowotny J, Sorrell CC, editors. Electrical properties of oxide materials. Enfield, NH: Trans Tech Publ, 1997, p. 1.
[73] Finklea HO. In: Finklea HO, editor. Semiconductor electrodes. Amsterdam: Elsevier, 1988. p. 1–145.
[74] Gerischer J. In: Seraphin BO, editor. Solar energy conversion. Berlin: Springer, 1979. p. 115–72.
[75] Nakato Y, Obnishi J, Tsobomura H. Chem Lett 1975;883:2.
[76] Wrighton MS, Austin RG, Bocarsly AB, Bolts JM, Haas O, Legg KD, Palazzotto MC. J Am Chem Soc 1978;100:1602.
[77] Bolts JM, Bocarsly AM, Palazzotto MC, Walton EG, Lewis NS, Wrighton MS. J Am Chem Soc 1979;101:1378.
[78] Skotheim T, Lundstrom I, Preja J. J Electrochem Soc 1981;128:1625.
[79] Ghosh AK, Muruska HP. J Electrochem Soc 1977;124:1516.
[80] Haneman D, Steenbeeke F. J Electrochem Soc 1977;124:861.
[81] Houlihan JF, Armitage DB, Hoovler T, Bonaquist D, Madacsi DP, Mulay LN. Mater Res Bull 1978;13:1205.
[82] Maruska HP, Ghosh AK. Sol Energy Mater 1979;1:237.
[83] Blondeau G, Froelicher M, Froment M, Hugot-Le Goff A, Zerbino J. J Electrochem Soc 1979;126:1592.
[84] Rauh RD, Buzby JM, Reise TF, Alkallis SA. J Phys Chem 1979;83:2221.
[85] Guruswamy V, O'M Bockris J. Sol Energy Mater 1979; 1:441.
[86] Stadler C, Augustynski J. J Electrochem Soc 1979;126:2007.
[87] Campet G, Verniolle J, Doumerc JP, Claverie J. Mater Res Bull 1980;15:1135.
[88] Salvador P. Sol Energy Mater 1980;2:413.
[89] Salvador P. Mater Res Bull 1980;15:1287.
[90] Monnier A, Augustynski J. J Electrochem Soc 1980; 127:1576.
[91] Matsumoto Y, Kurimoto J, Yamagasaki, Sato E. J Electrochem Soc 1980;127:2148.
[92] Claverie J, Verniolle J, Campet G, Doumerc J-P, Hagenmuller H. Mater Res Bull 1981;16:1019.
[93] Matsumoto Y, Kurimoto J, Yamagasaki, Sato E. J Electrochem Soc 1981;128:1040.
[94] Salvador P. Sol Energy Mater 1982;6:241.
[95] Giordano N, Antonucci V, Cavallaro S, Lembo R, Bart JCJ. Int J Hydrogen Energy 1982;7:867.
[96] Matsumoto Y, Shimizu T, Toyoda A, Sato E. J Phys Chem 1982;86:3581.
[97] Danzfuss B, Stimming U. J Electroanal Chem 1984;164:89.
[98] Herrmann JM, Disdier J, Pichat P. Chem Phys Lett 1984;108:618.
[99] Gutierrez C, Salvador P. J Electroanal Chem 1985;187:139.
[100] Prasad G, Chandra Babu KS, Srivastava ON. Int J Hydrogen Energy 1989;14:537.
[101] Kutty TRN, Avudaithai M. Chem Phys Lett 1989;163:93.
[102] Chandra Babu KS, Srivastava ON. Int J Hydrogen Energy 1989;14:529.
[103] Kutty TRN, Avudaithai M. Int J Hydrogen Energy 1990;15:621.
[104] Chandra Babu KS, Singh D, Srivastava ON. Semicond Sci Technol 1990;5:364.
[105] Wang CM, Mallouk TE. J Phys Chem 1990;94:423.
[106] Kikkawa K, O'Regan B, Anderson MA. J Electroanal Chem 1991;309:91.
[107] Chandra Babu KS, Singh D, Srivastava ON. Int J Hydrogen Energy 1991;16:387.
[108] Choi W, Termin A, Hoffmann MR. J Phys Chem 1994;98:13669.
[109] Wang MH, Guo RJ, Tso TL, Preng TP. Int J Hydrogen Energy 1995;20:555.
[110] Guo RJ, Wang MH, Tso TL, Preng TP. Int J Hydrogen Energy 1995;20:561.
[111] Wang Y, Cheng H, Hao Y, Ma J, Li W, Cai S. Thin Solid Films 1999;349:120.
[112] Nakatano Y, Shioji M, Tsubomura H. Chem Phys Lett 1982;90:453.
[113] Reisfeld R, Eyal M, Brusilovsky D. Chem Phys Lett 1988;153:210.
[114] Malta OL, Couto dos Santos MA. Chem Phys Lett 1990;174:13.
[115] Zhao G, Kozuka H, Yoko T. Thin Solid Films 1996;277:147.
[116] Liao HB, Xiao RF, Wang H, Wong KS, Wong GKL. Appl Phys Lett 1998;72:1817.
[117] Gerischer H, Tribusch H. Ber Bunsenges Phys Chem 1968;72:1083.
[118] Gerischer H. Photochem Photbiol 1972;16:243.
[119] Memming R. Photochem Photbiol 1972;16:325.
[120] Matsumura M, Nomura Y, Tsobomura H. Bull Chem Soc Jpn 1977;50:2533.
[121] O'Regan B, Gratzel M. Nature 1991;353:737.
[122] Parkinson BA, Spitler AM. Electrochem Acta 1992;37: 943.

[123] El Zayat MY, Saed AO, El-Dessouki MS. Int J Hydrogen Energy 1998;23:259.
[124] Bak T, Nowotny J, Rekas M, Sorrell CC. Int J Hydrogen Energy 2001;27:19.
[125] Bak T, Nowotny J, Rekas M, Sorrell CC. Int J Ionics 2001;7:272.
[126] Archer MD, Bolton JR. J Phys Chem 1990;94:8028.
[127] Parkinson B. Acc Chem Res 1984;17:431.
[128] Barin I. Thermochemical data of pure substances, part I. Weinheim: VCH Verlagsgeselschaft mbH, 1989. p. 796.
[129] Bolton JR, Strickler SJ, Connolly JS. Nature 1985;316: 4945.
[130] Okuda M, Yoshida K, Tanaka N. Jpn J Appl Phys 1976;15:1599.
[131] Laser D, Bard AJ. J Electrochem Soc 1976;123:1027.
[132] Guruswamy V, Murphy OJ, Young V, Hildreth G, O'M Bockris J. Sol Energy Mater 1981;6:59.
[133] Yoon KH, Kim TH. J Solid State Chem 1987;67:359.
[134] Akikusa J, Khan SUM. Int J Hydrogen Energy 1997;22:875.
[135] Parkinson BA, Heller A, Miller B. Appl Phys Lett 1978; 33:521.
[136] Nakatani K, Matsud M, Tsumobura H. J Electrochem Soc 1978;125:406.
[137] Wrighton MS, Bocarley AB, Bolts JM, Ellis AB, Legg KD. In: Heller A, editor. Semiconductor liquid junctions solar cells. The Electrochemical Society, Perington, NJ. 1977. p. 138.
[138] Thomas CE, James BD, Lomax Jr FD. Market penetration scenarios for fuel cell vehicles. Int J Hydrogen Energy 1998;23:949.
[139] The Daily Yomiuri (Japan), 18 August 2001.
[140] Kofstad P. Nonstoichiometry, electrical conductivity and diffusion in binary metal oxides. New York: Wiley, 1972.
[141] Bak T, Nowotny J, Rekas M, Sorrell CC, Kuratomi T, Yamaguchi K, Yamawaki M. Solid State Ionics, in print.
[142] Tai W-P. Mater Lett 2001;51:451–4.
[143] Becquerel E. Compt Rendues 1839;9:561.
[144] Brattain WH, Garret CG. Phys Rev 1954;94:750.
[145] Brattain WH, Garret CG. Bell System Techn J 1955;34:129.
[146] Gerischer H. Z Phys Chem 1960;26:223.
[147] Memming R. J Electroanal Chem 1969;11:785.
[148] Williams A. US Patent Number US 1983000523251 (21 August 1983).
[149] Appelby AJ. US Patent Number 4,643,817 (17 February 1987).
[150] Miller E, Rochleau R. Energy Fuels 1998;12:3.